AD-A091 752 WISCONSIN UNIV-MADISON SPACE SCIENCE AND ENGINEERING --ETC F/G 4/2
STUDIES IN OBJECTIVE FORECASTING OF MESOSCALE WEATHER USING AN --ETC(U)
JUN 80 C H WASH, R O'KEEFE, T M WHITTAKER F19628-78-C-0137
UNCLASSIFIED SCIENTIFIC-2 AFGL-TR-80-0309 NL

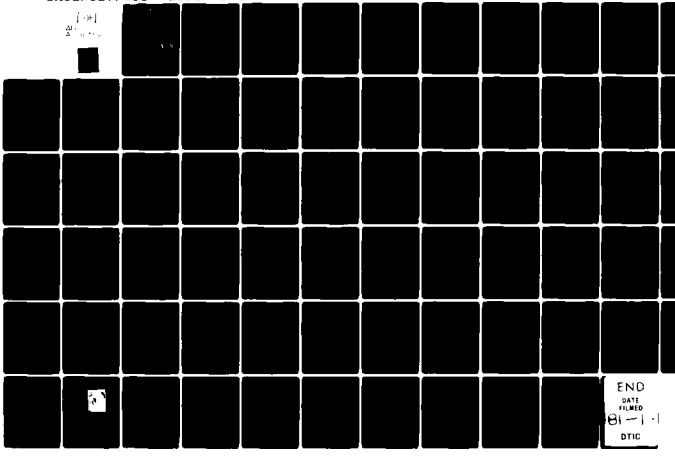

END
DATE FILMED
81-1-1
DTIC

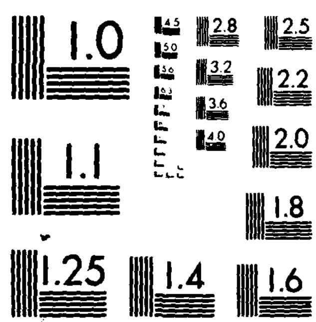

MICROCOPY RESOLUTION TEST CHART
NATIONAL BUREAU OF STANDARDS-1963-A

AFGL-TR-80-0309

LEVEL II (12)

STUDIES IN OBJECTIVE FORECASTING OF MESOSCALE WEATHER USING AN INTERACTIVE COMPUTER SYSTEM

Carlyle H. Wash
Raymond O'Keefe
Thomas M. Whittaker
Delain A. Edman
Donald R. Johnson

Space Science & Engineering Center
University of Wisconsin
1225 West Dayton Street
Madison, Wisconsin 53706

AD A091752

15 June 1980

DTIC
ELECTE
S NOV 18 1980 D
A

Scientific Report No. 2

Approved for public release; distribution unlimited

DDC FILE COPY

AIR FORCE GEOPHYSICS LABORATORY
AIR FORCE SYSTEMS COMMAND
UNITED STATES AIR FORCE
HANSCOM AFB, MASSACHUSETTS 01731

80 11 17 075

Qualified requestors may obtain additional copies from the Defense Technical Information Center. All others should apply to the National Technical Information Service.

Unclassified

SECURITY CLASSIFICATION OF THIS PAGE (When Data Entered)

(19) REPORT DOCUMENTATION PAGE	READ INSTRUCTIONS BEFORE COMPLETING FORM
(18) 1. REPORT NUMBER: AFGL-TR-80-0309	2. GOVT ACCESSION NO.: AD-A091 752	3. RECIPIENT'S CATALOG NUMBER
(6) 4. TITLE (and Subtitle): STUDIES IN OBJECTIVE FORECASTING OF MESOSCALE WEATHER USING AN INTERACTIVE COMPUTER SYSTEM	(9) 5. TYPE OF REPORT & PERIOD COVERED: Annual Report 15 June 1979 — 15 June 1980
	6. PERFORMING ORG. REPORT NUMBER: Scientific Report Number 2
(10) 7. AUTHOR(s): Carlyle H. Wash, Delain A. Edman, Raymond O'Keefe, Donald R. Johnson, Thomas M. Whittaker	(15) 8. CONTRACT OR GRANT NUMBER(s): F19628-78-C-0137
9. PERFORMING ORGANIZATION NAME AND ADDRESS: Space Science & Engineering Center, Univ. of Wis. 1225 W. Dayton Street Madison, WI 53706	10. PROGRAM ELEMENT, PROJECT, TASK AREA & WORK UNIT NUMBERS: 62101F (16) 667008AB (17) 08
11. CONTROLLING OFFICE NAME AND ADDRESS: Air Force Geophysics Laboratory (11) Hanscom Air Force Base, MA 01731 Monitor/R. S. Hawkins/LYU	12. REPORT DATE: 15 June 1980
	13. NUMBER OF PAGES: 78
14. MONITORING AGENCY NAME & ADDRESS (if different from Controlling Office): (12) 75	15. SECURITY CLASS. (of this report): Unclassified
	15a. DECLASSIFICATION/DOWNGRADING SCHEDULE

16. DISTRIBUTION STATEMENT (of this Report)

Approved for public release; ~~distribution unlimited~~

(14) SCIENTIFIC-2

17. DISTRIBUTION STATEMENT (of the abstract entered in Block 20, if different from Report)

18. SUPPLEMENTARY NOTES

A portion of this report is to be published in the Bulletin of the American Meteorological Society.

19. KEY WORDS (Continue on reverse side if necessary and identify by block number)

Interactive Computer System, GOES Satellite Data, Weather Forecasting, Advection, Discriminant Analysis.

20. ABSTRACT (Continue on reverse side if necessary and identify by block number)

GOES satellite imagery was used in conjunction with surface hourly weather observations in order to ascertain the ability of the satellite data to discriminate thunderstorm occurrence in regions with some cloudiness. Research was also conducted to study the ability of a vertically-integrated wind field to correctly advect observed surface frontal features.

DD FORM 1 JAN 73 1473

406303

SECURITY CLASSIFICATION OF THIS PAGE (When Data Entered)

TABLE OF CONTENTS

LIST OF FIGURES

LIST OF TABLES

1. INTRODUCTION

This report describes nowcasting research conducted at Space Science and Engineering (SSEC) under an Air Force Geophysical Laboratory (AFGL) contract during the past year. The overall research objective is to develop methods of improving short-range terminal weather forecasting techniques though the use of McIDAS (Man-computer Interactive Data Access System) for the processing and application of satellite and conventional meteorological data. Primary emphasis is placed on specifying and forecasting weather features such as ceilings, visibility, precipitation and also rarer events such as severe storms and turbulence.

McIDAS, the key tool in this research, permits rapid access and display of various types of meteorological data (satellite, surface, radiosonde and radar). Its capabilities include the real time input of digital satellite data, display of satellite images with accurate latitude and longitude gridding, enhancement of any portion of the brightness range and computations with the brightness data. In addition, surface and radiosonde data are available in plotted or analyzed form on either latitude-longitude or satellite map projections. Fields of atmospheric structure and dynamical processes can also be displayed. The system provides for the rapid integration of conventional and satellite data and also facilitates computation of simple diagnostic and forecast algorithms. For more details on the McIDAS system, the reader is referred to Hilyard,[1] Chatters and Suomi[2] and Smith[3].

---

1. Hilyard, J., editor, 1977: Interactive Video Displays for Atmospheric Studies. Proceedings of a workshop at the University of Wisconsin, Madison, 14-16 June, 1977.
2. Chatters, G.C. and V. E. Suomi, 1975: The application of McIDAS. IEEE Trans. Geosci. Electron., GE-13, 137-46.
3. Smith, E. A., 1975: The McIDAS system. IEEE Trans. Geosci. Electron., GE-13, 123-136.

The year's work supported by this contract focused on two research objectives:

1. the development of objective methods for detecting and monitoring subsynoptic and mesoscale regions of adverse weather, and
2. the development of algorithms for the short range prediction of frontal zones and adverse weather areas using advection and extrapolation.

The research initiated under the first objective focused on the application of GOES digital data to quantitatively delineate and forecast movement of convective weather areas. Using McIDAS, collocated surface and digital satellite data were collected during periods of enhanced convective activity. Discriminant analysis and regression techniques were applied to this data set to investigate the ability of GOES digital brightness statistics to isolate convective activity.

Work under the second objective emphasized the development and testing of an advective algorithm for the short-range prediction of frontal zones and other surface features. The advection technique uses a steering current determined from a density-weighted vertical average of the tropospheric wind field. Detailed verification of two test cases are presented and discussed.

In Chapter 2, statistical brightness studies are described while the advective algorithm development is outlined in Chapter 3. Brightness extrapolation procedures were discussed in last year's report[4] and will not be addressed.

---

4. Wash, C. H., T. M. Whittaker, and D. R. Johnson, 1979: Initial Studies in objective forecasting of mesoscale weather using interactive computer system. Scientific Report No 1, Air Force Geophysics Laboratory, 18 pp.

2. STATISTICAL BRIGHTNESS STUDIES

The goal of this effort is the objective determination of subsynoptic and mesoscale regions of adverse weather from satellite derived statistics. The primary source of information for this determination is the visible and infrared data from GOES. Considerable effort has already been expended in the development of operational nephanalysis procedures from satellite data in order to specify cloud type and coverage. Currently the Air Force employs both DMSP and NOAA visual and infrared (IR) satellite data as well as conventional weather data as input to an operational nephanalysis system (Fye[5]). An example of another objective nephanalysis procedure using DSMP visual and IR digital data is presented by Harris and Barrett[6].

Closely associated with objective nephanalysis is objective weather forecasting in the 0- to 6-h time period (short-range). Several authors have investigated the feasibility of using statistical models with satellite data as input to predict short-range weather. Sikula and Vonder Haar[7] used satellite statistics derived from ATS-3 data to show that ceiling and cloud cover can be predicted with skill over persistence at periods greater than two hours. Muench and Keegan[8] investigated techniques designed to specify cloud cover and precipitation rates from satellite data in addition to automated

---

5. Fye, F. K., 1978: The AFGWC automated cloud analysis model. AFGWC Technical Memorandum 78-002, Air Force Global Weather Central, 97 pp.
6. Harris, R., and E. C. Barrett, 1978: Toward an objective nephanalysis. J. Appl. Meteor., 17, 1258-1266.
7. Sikula, G. J., and T. H. Vonder Harr, 1972: Very short range local area weather forecasting using measurements from geosynchronous meteorological satellites. Colorado State Univ. Atmospheric Science Paper No. 185, Air Force Contract No. F19628-71-C-0073, 73 pp.
8. Muench, H. S., and T. J. Keegan, 1978: Automated short-range forecasting of cloud cover and precipitation using geo-synchronous satellite imagery data. Preprints Eighth Technical Exchange Conf., Colorado Springs, 113-117.

forecasting techniques using cloud pattern extrapolation. Negri, et al.[9] related reflected brightness values to a precipitation/no precipitation threshold, and also suggested that satellite derived growth rates may be an effective parameter in determining storm severity. Adler and Fenn[10,11] extended the work of Negri et al. by relating thunderstorm growth rates to vertical velocity and outflow layer divergence. Their results indicated that severe thunderstorms have mean vertical velocities twice as large as non-severe thunderstorms. Zak[12] presented an excellent analysis of statistical methods used for thunderstorm forecasting over the 2- to 6-h period.

In spite of the important gains made in objective nephanalysis during the past decade, a problem remains before nephanalysis output can be incorporated into objective forecasting schemes. A nephanalysis only determines the cloud amount and type, not the weather occurring below the clouds. An objective forecast predicts the weather (thunderstorm, snow, fog, etc.) and attendant variables (wind, visibility, temperature, etc.). For forecast needs, a method based on nephanalysis should be developed to specify weather type and severity from satellite information. An attempt to address this problem through development of a technique for weather specification based on satellite statistics is now described.

---

9. Negri, A. J., D. W. Reynolds, and R. A. Maddox, 1976: Measurements of cumulunimbus clouds using quantitative satellite and radar data. Preprint Volume of Seventh Conference on Aerospace and Aeronautical Meteorology, Melbourne, 119-124.
10. Adler, R. F., and D. D. Fenn, 1979a: Satellite-based thunderstorm intensity parameters. J. Appl. Meteor., 18, 502-517.
11. Adler, R. F., and D. D. Fenn, 1979b: Thunderstorm vertical velocities estimated from satellite data. J. Atmos. Sci., 36, 1747-1754.
12. Zak, J. A., 1977: Forecasting thunderstorms over a 2- to 5-h period by statistical methods. NASA Contractor Report 2934, 112 pp.

Although the methodology presented here is for a specific weather event, the approach is general enough to be applied to any weather event. The immediate goals are the objective determination of the presence of thunderstorm(s) within a user specified area and its severity given the presence of a thunderstorm. The predictors for this study will be satellite derived statistics and the ground truth will be the airways surface reports.

2.1 Data aquisition.

The initial plans for the acquisition of a data base called for totally automated procedures because of the large amounts of satellite data transmitted and the savings in time and money gained from automation. However, due to unforseen changes in staff and equipment, our original plans were modified. A semi-automated data acquisition procedure using McIDAS was adopted which met the three basic requirements: 1) the system was able to process large quantities of data quickly and inexpensively; 2) to collocate surface synoptic reports with corresponding satellite data; and 3) to store this information on tape for future analysis.

2.1.1 Determination of optimum pixel matrix. A pilot study was undertaken to determine the optimum size pixel matrix of information to use about a station. In this study, two nautical-mile visible resolution was used in order to reduce computer storage space and to obtain information over a larger surface area than would have been possible if one nautical-mile resolution was used. The two nautical-mile resolution also provides for consistent spatial resolution in both the visible and IR images. The study was accomplished with data from May 1978 and carried out at the McIDAS user terminal in order to allow for maximum human input into this important question. In the pilot study, thirteen randomly selected thunderstorm events from two hours of data

were selected, as were 16 no-thunderstorm events. No corrections of the data were made for sun angle, anisotropy, and navigation errors in the pilot study. Visible and IR statistics (the mean for both spectral channels) were computed for pixel sizes of 6 x 6 (36 points), 10 x 10 (100 points), and 20 x 20 (400 points). Plots of mean visual vs. mean IR values were made. These plots are shown in Fig. 1. Despite the remarkable success of the 6 x 6 matrix in discriminating between thunder and no thunder, the 10 x 10 matrix (later increased to 11 x 11 in order to center the station) was chosen as the optimum size matrix. The decision to accept the 10 x 10 array in lieu of the 6 x 6 array was based on the fact there is approximately a 15 minute lag between the time of surface observation and satellite scan in mid-latitudes. Any thunderstorm occurring over the station at the time of the surface observation could be outside the 6 x 6 matrix by the time of the satellite scan. The 20 x 20 array was rejected because of its poor discriminating capabilities and its large computer storage requirements.

2.1.2 Data collection system. The semi-automated data acquisition plan consisted of the following operations performed in sequence:

1. The morning (0830Z) National Weather Service convective weather outlook for the United States was subjectively scanned for the possibility of general thunderstorm activity in the data gathering region (70W-105W, 30N-48N).
2. If the possibility of general thunderstorm activity existed, the data gathering program on McIDAS was initiated with a user-supplied key-in.
3. The McIDAS program performed the following procedures:
   a. scanned hourly airways reports for the presence of BKN or OVC skies;

b. obtained an 11 x 11 pixel matrix of GOES visible and IR data for current hour and previous half hour centered on station. A schematic diagram of the data storage arrangement is shown in Fig. 2.;

c. data from 3.a and 3.b was saved on McIDAS file until it could be read onto tape.

4. The program could operate for any four specified hours.

5. Data collected was read onto tape by a user-supplied key-in.

Through this acquisition system, thirty-four hours of data were collected between 18 April 1980 and 7 June 1980.

2.2 Data preparation.

Before the data could be statistically analyzed on the UNIVAC 1180, it was necessary to change the data from the McIDAS Harris/6 computer 24-bit word to the UNIVAC computer 36-bit word. Four data preparation steps were then performed. The steps were 1) correcting the satellite data for navigation errors and checking the data for stability; 2) normalizing the visual data for sun angle effects; 3) deleting observations containing missing data; 4) stratifying the data into dependent and independent samples.

Given two identical satellite images, data stability is defined as the ability of the satellite sensor to record identical brightness information from the two images. Keegan[13] reported that the stability of the GOES visual data was excellent. The dependent and independent samples were stratified by geography, while the thunderstorm events in the dependent and independent samples were stratified by severity.

---

13. Keegan, T. J., 1978: Variation in groud brightness over the northeastern United States as sensed by GOES satellites. AFGL-TR-78-0290, 20 pp.

The normalization of visual satellite data for sun angle is a complicated problem. Mosher[14] notes that the reflected light from horizontally homogeneous clouds depends on four variables. They are:

1. Drop size distribution and phase state of water particles,
2. Number density of scattering particles in the cloud,
3. Cloud thickness,
4. Zenith angles of the sun and the sensor, and their relative azimuth angle.

All variables except the solar zenith angle were neglected. This action has the effect of treating all clouds as isotropic or Lambertian reflectors. This assumption is valid for thick clouds and small (+30° to -30°) zenith angles (Sikdar and Suomi[15]). With these possible sources of error in mind, the normalization relation is defined by

$$B_{new} = (B_{old}) \sec z \quad , \qquad (1)$$

where

B_{new} - transformed brightness count ,

B_{old} - original brightness count ,

sec z - secant of solar zenith angle .

---

14. Mosher, F. R., 1973: Cloud brightness contrasts as viewed by a satellite. M.S. Thesis, University of Wisconsin-Madison, 60 pp.
15. Sikdar, D. N., and V. E. Suomi, 1972: On the remote sensing of mesoscale tropical convection intensity from a geostationary satellite. J. Appl. Meteor., 11, 37-43.

The secant of the solar zenith angle is given by

$$\sec z = (\sin \phi \sin \delta + \cos \phi \cos \delta \cos H)^{-1} \quad , \qquad (2)$$

where

ϕ - latitude ,

δ - solar declination angle ,

H - hour angle .

The solar declination was obtained from The Nautical Almanac: The hour angle was determined from

$$H = (SN - OH)*15 \quad , \qquad (3)$$

where

OH - observation hour ,

SN - solar noon determined by,

$$SN = 12. - \frac{(\lambda_S - \lambda)}{15} - \frac{EOT}{60} \qquad (4)$$

λ_S - standard longitude defined to be 75° for Eastern time, 90° for Central time, and 105° for Mountain time,

λ - longitude,

EOT - equation of time given by Astronomical Phenomena For the Year 1980.

The hour angle is measured in degrees. Typical correction factors (sec z) for selected locations and times are presented in Table 1.

Table 1

Normalization Factors (sec z)

Date and Time	Station JFK	MIA	ORD	HOU	DEN
4/18, 19Z	1.32	1.13	1.20	1.07	1.15
5/12, 21Z	1.84	1.62	1.38	1.21	1.21
6/7, 15Z	1.15	1.18	1.37	1.42	1.64

Observations which contained missing satellite data were deleted from further consideration in the study.

At this point in the data processing routine, the data were considered to be and ready for analysis. A summary of the data set is presented in Table 2.

Table 2

Summary of Data Set

Data set #	Date	Time(s)	Total # Stations	Total # Good STA	Reported Weather T[1]	H	F	K	R[2]	Other Weather[3]
1	4/24	18-21Z	753	741	9	34	6	0	39	653
2	5/12	19,21,22Z	925	578	16	42	31	0	55	434
3	5/27	19-22Z	819	373	11	43	0	1	5	310
4	5/29	17-20Z	846	839	37	196	21	1	36	549
5	5/29	23Z	183	132	6	25	5	0	9	87
6	5/30	12Z,13Z	371	358	5	95	86	1	30	142
7	5/30	18Z	246	243	8	57	9	0	15	154
8	6/4	17-20Z	630	615	16	30	6	2	9	556
9	6/5	17,19,20Z	579	560	10	75	20	0	23	432
10	6/7	15,16,18 20Z	1141	1133	37	180	89	0	73	754
TOTAL	8	34	6493	5570	155	774	273	5	294	4071

[1] Includes T, TRW-, TRW, TRW+, TR-, TR, and TR+
[2] Includes RW-, RW, RW+, R-, R, and R+
[3] Includes all other weather events not listed

2.2.1 Data stratification. The first stratification divided the observations into either a dependent or independent sample through the use of a pseudo-random number routine supplied by MACC[16]. With the desire to place approximately eighty percent of the observations from each category into a dependent sample, each observation was assigned an identification number (1 to 155 for the thunderstorm cases and 1 to 5415 for the no thunderstorm cases). By generating about twice as many random numbers as observations for each category, and placing those events whose identification numbers were (randomly) chosen more than once into the dependent samples, the goal was achieved. The dependent thunderstorm sample consisted of 85% of the total thunderstorm observations, while the dependent no thunderstorm sample contained 83% of the total no thunderstorm observations. The independent samples consisted of the remainder in each category.

Next, the dependent and independent samples were stratified by geography. This stratification was based on the map shown in Fig. 3. Finally, the thunderstorm observations were stratified by severity. The results of these stratifications are presented in Table 3.

---

16. Madison Academic Computing Center, 1978: Random Number Routines. Reference Manual, University of Wisconsin-Madison, 79 pp.

Table 3
Geographical Stratification

		SAMPLE			
		Dependent		Independent	
		T#	no-T*	T#	no-T*
GEOGRAPHICAL LOCATION	NE	8	895	1	169
	SE	29	1259	8	252
	MID	81	1754	13	382
	MOUNT	13	579	2	127

#T -- Thunderstorm
*no-T -- No Thunderstorm

Severity Stratification

		SAMPLE	
		Dependent	Independent
SEVERITY	THUNDER[1]	37	6
	LIGHT THUNDER SHOWER[2]	70	15
	HEAVY THUNDER SHOWER[3]	24	3

[1] Thunder -- T

[2] Light Thunder Shower -- TRW-, TR-

[3] Heavy Thunder Shower -- TRW, TR, TRW+, TR+

2.3 Data analysis and results

The basic question to be addressed in this section is whether two or more sample groups are members of a single multivariate population or of two or more multivariate populations. The first goal, thunderstorm determination, requires a means to discriminate between two populations--thunderstorm/no thunderstorm, while the second goal, thunderstorm severity, requires a means to discriminate among three populations. A variety of statistics to be determined from the data were selected for candidate predictors for the statistical models. These candidate statistics are summarized in Table 4 along with their meteorological relationships.

2.3.1 Regression analysis. Research performed on the full dependent data set using regression analysis to discriminate between thunderstorms and no thunderstorms yielded poor results. When a dichotomous dependent variable (0-no thunderstorm, 1-thunderstorm) is used in regression analysis, the resulting mean response is the probability that the indicator variable equals one (Neter and Wasserman[17]). Fifteen (variables 1, 2, 3, 4, 23 and 24 as listed in Table 4) linear, two-dimensional regression models were produced using a dichotomous dependent variable. The data was categorized to compare regression analysis results with discriminant analysis results. All mean responses greater than 0.5 were assigned to the thunderstorm group, and all mean responses less than 0.5 were assigned to the no-thunderstorm group. For all models, the regression equations failed to detect a single thunderstorm on the basis of the 0.5 criterion. There are two possible explanations why the regression analysis failed. First, regression model assumptions of normally distributed error

---

17. Neter, J., and W. Wasserman, 1974: Applied Linear Statistical Models. Richard D. Irwin, Inc., 842 pp.

Table 4

Statistical Predictors and Meteorological Relation

Note: All statistics are determined from an 11 x 11 pixel matrix (121 points)

Predictor #	Predictor	Predictor Symbol	Meteorological Relevance
1,2	Mean IR[1]	$\overline{B}_{IR}$, $\overline{B2}_{IR}$	average temperature in field of view (FOV)
3,4	Mean visible[1]	$\overline{B}_V$, $\overline{B2}_V$	average albedo in FOV
5,6	Standard deviation IR[1]	SD_{IR}, $SD2_R$	texture in FOV: high SD-rough; low SD-smooth
7,8	Standard deviation visible[1]	SD_V, $SD2_V$	texture in FOV: high SD-rough; low SD-smooth
9	$\overline{B}_{IR} - \overline{B2}_{IR}$	D_{IR}	temporal change in temperature in FOV
10	$\overline{B}_V - \overline{B2}_V$	D_V	temporal change in albedo in FOV
11,12	Max IR value[1]	MAXIR, MAXIR2	max height of object (cloud) in FOV
13,14	Min IR value[1]	MINIR, MINIR2	min height of object (cloud/ground) in FOV
15,16	Max visual value[1]	MAXV, MAXV2	max albedo of object (cloud/ground) in FOV
17,18	Min visual value[1]	MINV, MINV2	min albedo of object (cloud/ground) in FOV
19	MAXIR-MINIR	RANIR	texture in FOV: large range-rough
20	MAXIR2-MINIR2	RANIR2	texture in FOV: small range-smooth
21	MAXV-MINV	RANV	Texture in FOV: large range-rough
22	MAXV2-MINV2	RANV2	Texture in FOV: small range-smooth
23	$(\overline{B}_{IR}+\overline{B2}_{IR})/2$	$\overline{BM}_{IR}$	synchronize OB time with satellite scan time for average temperature
24	$(\overline{B}_V+\overline{B2}_V)/2$	$\overline{BM}_V$	in FOV and average albedo in FOV

[1] Includes calculations for current hour and previous half hour

terms and constant error variance were violated. Second, the ratio of thunderstorm cases to no-thunderstorm cases in the full dependent data set is approximately 1:35. Since this ratio is so large, the no-thunderstorm data may have overwhelmed the thunderstorm data, thereby rendering the thunderstorm information useless.

Initially, both discriminant analysis and regression analysis using binary dependent data were to be used to discriminate between thunder and no-thunder cases. Based on these convincing results, the use of regression analysis was abandoned in favor of discriminant analysis.

2.3.2 Mathematical introduction to discriminant analysis. Discriminant analysis, developed by R. A. Fisher, assigns an observation X of unknown origin to one of two or more groups on the basis of the value of the observation. Cooley and Lohnes[18] present a detailed derivation of the linear discriminant model. The salient features of their derivation are summarized here. The discriminant function is given by the linear combination

$$Y = C_1 x_1 + C_2 x_2 + \ldots + C_n x_n \qquad (5a)$$

or in vector form,

$$\underset{\sim}{Y} = \underset{\sim}{C}' \underset{\sim}{x} \quad , \qquad (5b)$$

where $\underset{\sim}{C}'$ represents the transpose of the coefficient vector, and $\underset{\sim}{x}$ represents the variable vector. The best discriminant function maximizes the

---

18. Cooley, W. W., and P. R. Lohnes, 1971: Multivariate Data Analysis. John Wiley and Sons, Inc., 364 pp.

ratio of the among groups sum of squares ($\underset{\sim}{A}$) to the within groups sum of squares ($\underset{\sim}{W}$), so that the among group differences will be large relative to the within group scatter. The basic vector equation of discriminant analysis is

$$\underset{\sim}{A}\,\underset{\sim}{v} = \lambda_j \underset{\sim}{W}\,\underset{\sim}{v} \qquad j = 1,\ldots,m \qquad (6)$$

where λ_j is the eigenvalue(s) and m is the number of discriminant functions. Premultiplying both terms by W^{-1} and rearranging terms, (6) becomes

$$(\underset{\sim}{W}^{-1}\underset{\sim}{A} - \lambda I)\underset{\sim}{v} = \underset{\sim}{0} \quad . \qquad (7)$$

The eigenvalue(s) is either zero or positive. The number of positive eigenvalues, and hence the number of discriminant functions is determined by the number of p predictors or g groups minus one whichever is smaller. Corresponding to each positive eigenvalue, there is a vector $b\underset{\sim}{C}$ which satisfies equation (7). Since b is an arbitrary constant, it is customary to normalize each of the coefficients by dividing them by the square root of the sum of the squares of all coefficients. After this has been accomplished, the best discriminant function is given by equation (5a). To investigate the first objective, only one discriminant function is needed since only two groups, thunderstorms and no thunderstorms, were to be discriminated. The second objective required two discriminant functions since three groups, thunder, heavy thundershowers, and light thundershowers, were to be discriminated.

All discriminant analysis calculations were made under the following two assumptions:

1. the p predictors are assumed to be from a multivariate normal distribution;
2. the group dispersion matrices (variance-covariance matrices) are equal.

Research by Lachenbruch, Sneering and Revo (Lachenbruch[19]) indicates that discriminant analysis is non-robust for departures from normality. Research performed by Marks and Dunn (Lachenbruch[20]) indicates that discriminant analysis is fairly robust to small differences among dispersion matrices.

A battery of several significance tests are available to test not only the validity of these assumptions, but also the adequacy of the final model. The validity of the normality assumption may be ascertained by plotting the data and inspecting it for departures from normality. The validity of equal dispersion matrices may be obtained from a test devised by Box (Cooley and Lohnes[21]). A test for equality of group means (a measure of the effectiveness of the discriminating function) is Wilks' Lambda test (Λ) using Rao's F-approximation (Cooley and Lohnes[22]). Rao's V-statistic (Schlater and Learn[23]) was the criterion for including variable(s) in the forward stepwise procedure used to derive the discriminant function.

---

19. Lachenbruch, P. A., 1975: Discriminant Analysis. Hafner Press, 128 pp.
20. Ibid.
21. Cooley, W. W., and P. R. Lohnes, 1971: Multivariate Data Analysis. John Wiley and Sons, Inc., 364 pp.
22. Ibid.
23. Schlater, J., and J. Learn, 1975: DISCRIM1: Discriminant Analysis. Academic Computing Center, University of Wisconsin-Madison, 55 pp.

2.3.3 Computational aspects of discriminant analysis. The discriminant analysis was completed using the STATJOB-DISCRIM 1 (Schlater and Learn[24]) package provided by MACC. The forward stepwise procedure used Rao's V-statistic as the criterion for including variables in the discriminant model. The stepwise algorithm proceeded in the following manner:

1. Assume the model is composed of p variables;
2. Further assume q additional variables were to be added to the model;
3. If Rao's V-statistic was significant at the critical level (0.10), the entire set of $p+q$ variables was included in the model. Otherwise, only the p variables were included in the model.

In this initial study emphasis was placed on simplicity, thus only candidate predictors 1, 2, 3, 4, 23 and 24 listed in Table 4 were chosen. This choice of predictors resulted in 15 possible two dimensional, linear discriminant models. The dependent data set consisted of 65 cases each, of randomly selected thunderstorm and no-thunderstorm events. An independent data set was also constructed consisting of 24 thunderstorm cases and 24 non-thunderstorm cases. Visual inspection of the data plots shown in Figs. 4a-o indicated that the assumption of multivariate normality was satisfied. Box's test was used to determine which of the models satisfied the assumption of equal dispersion matrices. The hypothesis tested was

$$H_0 : \Delta_1 = \Delta_2 = \ldots = \Delta_i = \Delta \quad , \quad i = 1, 2, \ldots, g$$

$$H : \text{all } \Delta_i \text{ not equal} \quad ,$$

---

24. Ibid.

where Δ is the dispersion matrix, and g is the number of groups. The significance level of the test was $\alpha = 0.05$. If the calculated significance level was greater than 0.05, H_0 was not rejected and the model was accepted. Otherwise, H_0 was rejected and the model was rejected. Seven models were rejected on the basis of unequal dispersion matrices leaving eight models available for analysis.

The accepted discriminant functions are shown in Figs. 5a-h. If $L > 0$ the observation is assigned to the thunderstorm group; if $L < 0$ the observation is assigned to the non-thunderstorm group; if $L = 0$ the observation has an equal probability of belonging to either group. All models were found to be highly significant with a significance level of $< 5 \times 10^{-5}$ as determined by Λ.

Several comments concerning the results of Figs 5a-h are in order.

1. Twelve of the 16 predictors chosen indicated the importance of a time lag predictor (i.e., $\overline{B2}_{IR}$, $\overline{B2}_{V}$, $\overline{BM}_{IR}$, $\overline{BM}_{V}$).
2. The importance of a time lag predictor in a model likely serves to explain the obvious absence of $\overline{B}_{V}$, and $\overline{B}_{IR}$ as predictors in a model.
3. On the basis Λ, for Figs. 4a-h, the mean statistic ($\overline{B}$ in all its forms) is judged to be a highly significant predictor. Among the 16 predictors listed for the eight models, eight were visible predictors and eight were IR predictors thereby suggesting the importance of multi-spectral information in classification.

While the plots of the data, discriminant functions and significance tests all show statistical significance, the presence of meteorological significance remains to be demonstrated. One method to estimate meteorological

significance is through the use of error rates. Lachenbruch[25] lists five different types of error rates. However, we will be concerned with only two of them--apparent error rate (apparent accuracy) and the actual error rates (actual accuracy). The apparent accuracy is the fraction of observations which are correctly classified by the discriminant function in the dependent sample, while the actual accuracy is the fraction of observations which are correctly classified by the discriminant function in the independent sample. These two accuracy measurements were chosen because their difference represents model bias (Riggio and Topham[26]), a bias that offers a criterion by which to compare the meteorological significance of each model. Apparent accuracy, actual accuracy, and bias for each of the eight models are listed in Table 5.

Table 5

Meteorological Significance of Each Model as Determined by Model Bias

Model Number	Apparent accuracy	Actual Accuracy	Model Bias
1	0.846	0.750	0.096
2	0.854	0.750	0.104
3	0.846	0.813	0.033
4	0.838	0.729	0.109
5	0.846	0.813	0.033
6	0.838	0.813	0.025
7	0.854	0.729	0.125
8	0.854	0.729	0.125

25. Lachenbruch, op. cit.
26. Riggio, R. F., and K. L. Topham, 1979: Using discriminant analysis to predict rainshower occurrence in the Texas HIPLEX area. Preprints Sixth Conf. on Prob. and Stat. in Atmos. Sci., Banff, 74-78.

Since the specification of no thunderstorms when thunderstorms were present in a region was considered to be a more serious error than the specification of thunderstorms when no thunderstorms were present, a test of model skill is presented as another evaluator of meteorological significance. The statistics used are probability of detection (proportion of thunderstorm events specified correctly), false alarm ratio (proportion of thunderstorm events specified incorrectly), no alarm ratio (proportion of thunderstorm events specified incorrectly), and critical success index (proportion of successful specifications of a thunderstorm event to the sum of the successful predictors and errors of both types) (Donaldson, et al.[27]). The determination of these statistics proceeds as follows:

1. Fig. 6 shows a diagram of a contingency table where w and x represent successes, y represents failure to detect a thunderstorm, and z represents failure to detect no thunderstorm

2. Probability of detection (POD) = $\frac{x}{x + y}$

   False alarm ratio (FAR) = $\frac{z}{x + z}$

   No alarm ratio (NAR) = 1 - POD

   Critical success index (CSI) = $\frac{x}{x + y + z}$.

3. The variable w is not included in the CSI because any index of success involving w would be very insensitive to x due to the larger number of non-thunderstorm cases than thunderstorm cases.

---

27. Donaldson, R. J., R. M. Dyer, and M. J. Kraus, 1975: An objective evaluator of techniques for predicting severe weather events. Preprints Ninth Conf. Severe Local Storms, Amer. Meteor. Soc., Norman, 321-326.

The results of this analysis for the eight models using independent data are presented in Table 6.

Table 6

Sensitivity of Models to Thunderstorm/No Thunderstorm Specification

Model Number	POD	FAR	NAR	CSI
1	.714	.167	.286	.625
2	.714	.167	.286	.625
3	.778	.125	.222	.700
4	.704	.208	.296	.594
5	.778	.125	.222	.700
6	.778	.125	.222	.700
7	.704	.208	.296	.594
8	.704	.208	.296	.594

Based on the evidence of Table 5 and Table 6, the following statements are made:

1. The models show definite skill when compared to no skill classification schemes. The skill scores for the independent data sample range from .729 to .813, while the skill scores for the no-skill classification schemes are .500 for all models.
2. Model bias statistics confirm the importance of temporal and spectral predictors in thunderstorm/no thunderstorm discrimination. Models with the lowest bias scores (3, 5, and 6) all contain $\overline{B2}_{IR}$ as the primary term, and either $\overline{B}_V$, $\overline{B2}_V$, or $\overline{BM}_V$ as the secondary term. Model 6 (lowest bias model), containing terms

$\overline{B2}_{IR}$ and $\overline{BM}_V$ as predictors, suggests two important concepts concerning thunderstorm determination: 1) since neither $\overline{B2}_{IR}$ nor $\overline{BM}_V$ represent the current hour satellite statistics, there is the likelihood that many thunderstorms move from the station locations to a position outside the 11 x 11 matrix by the time of the hourly satellite scan; 2) the IR and visible statistics are out phase in time, with the visible statistic ($\overline{BM}_V$) at observation time and the IR statistic ($\overline{B2}_{IR}$) 15 minutes prior to obseration time.

3. The results of Table 6 mirror the results of Table 5. Models 3, 5, and 6 perform the best when viewed in terms of POD, FAR, NAR, and CSI statistics, while models 4, 7, and 8 perform the worst when judged against these statistics.
4. The high actual accuracy rates indicate that IR and visual means derived from half-hourly satellite data provide an excellent first guess at the presence of a thunderstorm in a specified region.

Caution should be used in interpreting these results. The estimates come from small, equal sized (note that in the collected data there were almost 35 times as many non-thunderstorm cases as thunderstorm cases) samples.

2.4 Summary

A test study to determine the effectiveness of visual and infrared (IR) mean statistics derived from half hourly satellite data in specifying thunderstorms was completed. The Man-computer Interactive Data Access System (McIDAS) developed by the Space Science and Engineering Center (SSEC), University of Wisconsin-Madison was used to collect data for this study. Thirty-four hours of data were collected comprising over 6400 stations in

which 155 stations reported thunderstorms. The data set consisted of one line of Service-A information followed by four 11 x 11 matrices of satellite data. The 11 x 11 matrix size was chosen in order to maximize both discriminant potential and spatial coverage, and to minimize computer storage requirements.

The data were analyzed using a forward-stepwise discriminant analysis routine. Results of the data analysis procedure indicate that the mean visual and mean IR statistics provide an excellent first guess in the specification of thunderstorms in a limited region. Actual accuracies for eight linear discriminant models range from .729 to .813. Model results indicate the importance of both temporal and multi-spectral predictors in the discriminant function.

The positive results for the specification of thunderstorms from satellite data obtained in this study suggest that the method should be tested operationally. The algorithms developed for determination of thunderstorms would likely be applicable to other data bases if considerations are made for resolution and spectral bandwidth of the satellite sensors. In this study only a yes-no prediction of thunderstorm occurrence was made. For the prediction of thunderstorm occurrences utilizing the techniques developed in this study in other systems that employ data bases with similar resoluton and spectral bandwidths, the algorithms developed would likely require minimum modification. For systems with substantially different resolution and sensor characteristics, the algorithms are not likely to be readily transferable although the techniques would be applicable.

3. ADVECTIVE PREDICTION OF SURFACE FRONTAL FEATURES

Forecasting the movement of many meteorological features can be estimated by use of an advective or steering current. An integrated tropospheric wind field or fraction of the wind at some level is frequently utilized to determine the motion and future position of surface fronts and associated weather areas. This information is particularly valuable in the short-range forecast interval of 0-12 hours, the time period between the observed state and the National Meteorological Center's Limited Area Fine Mesh 12-hour forecast. The preparation of a short-range advective forecast is an excellent application of an interactive computer system that has access to upper air winds (to determine the advection), surface reports (to prepare mesoscale and final analyses), and radar and satellite data (to locate precipitation and thunderstorm lines and areas).

An area of research under this project is the development of an advective algorithm utilizing McIDAS to predict the short-term movement of fronts and frontal features as described by radar or satellite data. Langrangian method of advection used by Glahn, Lowry and Holdenbaugh[28] for the Techniques Development Laboratory's Sub-Synoptic Advective Model was found to be ideally suited for advective computations. The predicted grid point value is determined by moving along a backward trajectory determined by a characteristic or mean wind. A one-half hour time step is used in the trajectory computation. The predicted value at the grid point is then the value upstream at the end point of the backward trajectory. The end point position is a function of the

---

28. Glahn, H. R., D. A. Lowrey, and G. W. Hollenbaugh, 1969: An operational subsynoptic advection model. ESSA, Weather Bureau Tech. Memo WBTM-23, July, 1969.

length of the forecast and velocity of the characteristic wind. The scheme is a very time-efficient algorithm for advection computations.

Several methods can be used to determine the characteristic wind. Of the two approaches considered (one, a fraction of the velocity at a given level, e.g., one-half of 500 mb flow; and, two, a vertical average of the tropospheric wind field), the initial experiments clearly suggested a vertical average of the tropospheric wind was preferable. The most likely reason for this result is that weather phenomenon result from vertically-developed dynamical systems that move with the mean flow rather than one specific level.

A mean, density-weighted wind is defined by

$$\hat{\underset{\sim}{V}} = \frac{\sum_{i=1}^{n} \rho_i \underset{\sim}{V}_i}{\sum_{i=1}^{n} \rho_i}$$

where $\underset{\sim}{V}$ is the wind velocity and ρ is the density, while i is the index of the levels of a radiosonde report. This technique weights the low tropospheric winds more than the high tropospheric winds since density decreases with height. A simple average of the wind observations will be dominated by the high winds in the upper troposphere.

3.1 Program Description

Three separate advection program variations have been completed.

3.1.1 ADVECT/AFMESO. This program calculates the average and standard deviation of the parameter to be advected (in most cases surface temperature or moisture advection) at the initial hour. The program then advects an area

that has a higher value than some multiple of the standard deviation. The program calculates the advection by using four different lowest level bases for the computation of the mean wind. The intervals encompassed are the following:

SFC-500	1000-300	850-300	700-300
SFC-400	1000-250	850-250	700-250
SFC-300	1000-200	850-200	700-200
SFC-250	1000-150	850-150	700-150
SFC-200	1000-100	850-100	700-100

The program will calculate statistics for the whole grid or just a prescribed area. The output consists of printing the predicted field for all nine hours and corresponding statistical verification scores.

3.1.2 ADVECT-1/AFMESO. This version of the program uses the same techniques as above, except it advects actual grid point values. The results can be displayed on a line printer, or contoured on the display monitor. The display consists of 0, 3, 6 and 9 hour verification plots, the 3, 6 and 9 hour forecasts, and the mean wind field.

3.1.3 ADVECT-2/AFMESO. This version produces a time series of verification and forecast values for a specified point, using a mean wind selected for the forecast. Any number of locations (stations) can be selected for each test. The output consists of the advected value of the parameter and the new value of the initial input parameter for each hour of the forecast.

3.2 Results.

To test the algorithm two frontal forecast cases were examined in detail. The objective of the tests was to determine the effectiveness of the advection technique and to evaluate the nature of the characteristic wind

fields using different vertical limits. Studies of active weather situations indicated that surface temperature advection ($-\underset{\sim}{V}\cdot\nabla T$), computed by McIDAS from surface data, provided a distinct signature of surface frontal features. The goal of this experiment was to extrapolate the surface temperature advection field, noting in particular the movement of the axis of maximum advection which is the signature of the frontal zone. The advective algorithm can not intensify or weaken the predictive field, so that the prediction of the axis of the fronts is more important than differences in values between the predicted and observed fields.

3.3 April 5 1979 case.

A complex and difficult forecast situation was present over the Midwest on 5 April 1979. Figure 7 compares the 1200 GMT NMC surface analysis of the synoptic scale with the more detailed McIDAS subsynoptic surface analyses over the Midwest. The NMC surface analysis (Figure 7A) portrays what appears to be a routine front moving through the Midwest region. The more detailed analyses of surface data reveal the additional complexity of the situation Although objective streamlines (Figure 7B) show a distinct wind shift along the cold front, the analyses of surface temperature and surface temperature advection (Figure 7C) show a second front with a distinct maximum in surface temperature advection in the Dakotas to the northwest of the larger-scale front. GOES IR satellite data (Figure 7D) shows two cloud areas, one associated with each front. More detail on the McIDAS analysis of this frontal situation is presented in Wash and Whittaker[29].

---

29. Wash, C. H., and T. M. Whittaker, 1980: Subsynoptic Analysis and Forecasting with an Interactive Computer System. Accepted for publication in Bulletin of the AMS.

The major weather event of the day was the rapid advance of the secondary front through the Midwest. This front was characterized by a strong temperature gradient (20°C/300 km) and an intense but narrow temperature advection zone with maximum advection of -60°C/day or -2.5°C/hour. The weather associated with the front was quite dramatic. Strong sustained winds of 30-40 knots with gusts to 60-70 knots, intense snow squalls and temperature drops of 8°C to 12°C in two hours were common. The key meteorological forecast problem in this case was the arrival time of this intense secondary front over locations in the Midwest. Given accurate forecast positions of the front using McIDAS, specific short-range forecasts of high winds, low visibility, precipitation and temperature change could be made.

The value of the advective forecast algorithm in forecasting movement of this intense secondary front was explored. The experiments focused on using the advective model to make forecasts from the 1200 GMT data for the frontal movement during the day. The surface temperature advection field produced a distinct maximum which provided a signature of the location of the second front and associated frontal weather that was useful for forecasting the movement of the feature. Since the scheme is conservative, it did not account for any weakening or strengthening of the field.

3.3.1 Forecast pattern results. An example of frontal forecast in this case is presented in Figure 8. The density-weighted wind field from the 1200 GMT radiosondes was used to project the movement of secondary front from its initial location in North Dakota south and eastward across the upper Midwest. The limits of vertical integration used to determine the steering current are flexible. For this example, the limits were chosen to be 850 mb to 300 mb. The advective 3-, 6-, and 9-h forecasts is displayed in panels A, C and E of

Figure 8 with verifying 1500, 1800 and 2100 GMT analyses on panels B, D and F. The advective scheme correctly indicates southeastward movement of the frontal zone during the forecast period. The axis of maximum advection is denoted by heavy dashed lines in Figure 8. Comparison of the axis forecasts with verifying analyses indicates the advection algorithm provides a useful forecast of axis movement through the upper Midwest. Even at the nine-hour mark, the forecast axis of maximum advection (north central Wisconsin, southern Iowa, southern Nebraska) is within 100 km of that observed. The intensification of the advection field during the day which follows from the cyclogenesis to the northeast and the stronger temperature gradient across the front during daylight hours was not forecastwith this scheme.

3.3.2 Verification statistics. A second aspect to the verification was the calculation of areal threat scores to evaluate the accuracy of forecasting the maximum advective areas and to intercompare various limits of integration. The scores computed are the following:

$$\text{Threat Score} = \frac{A_C}{A_F + A_O - A_C}$$

$$\text{Bias} = A_F/A_O$$

$$\text{Post Agreement} = A_C/A_F$$

where A_C = area correct

A_O = area observed

A_F = area forecast

3.3.3 Verification results. The statistical scores for the forecasts of the advection region exceeding one standard deviation of the field (10.8°C/day) found in Figure 8 are:

Hour 3	Threat Score	.4706
	Bias	.8182
	Post Agreement	.7111
Hour 6	Threat Score	.3978
	Bias	.6667
	Post Agreement	.7115
Hour 9	Threat Score	.3438
	Bias	.5542
	Post Agreement	.7174

The bias statistic emphasizes the size of the forecast area as compared to the verification area and shows the basic problem that was encountered in this particular forecast. By 9 hours, the forecast area was almost one-half the size of the observed area. This factor clearly indicates the reason for the relatively low threat score by 9 hours. If the areas would have been approximately the same size, the threat scores would have been in the .5 to .6 range at 9 hours. Related to this, note that the Post Agreement, which is the percentage of forecast area predicted correctly, remains over 70% through the 9 hour period.

A number of combinations of lower and higher levels were tested to determine the best steering wind in this case. The lower level ranged from surface to 700 mb while the upper level ranged from 300 mb to 100 mb. The results are presented in Table 7.

Two methods were used to determine the best interval for advection. The first consisted of studying the program statistics. The statistics show

Table 7

Threat Scores for Advective Forecasts
From 1200 GMT 5 April 1979

	SFC-400	SFC-500	SFC-200	SFC-250	SFC-300
3	.3871	.4211	.4362	.4105	.4194
6	.3241	.2661	.3786	.3786	.3491
9	.3056	.2328	.3551	.3524	.3491

	1000-100	1000-150	1000-200	1000-250	1000-300
3	.4167	.4082	.4211	.4362	.4348
6	.4327	.3942	.3810	.3810	.3945
9	.3611	.3578	.3148	.3619	.3365

	850-100	850-150	850-200	850-250	850-300
3	.4040	.4211	.4167	.4211	.4255
6	.3925	.3846	.3810	.3750	.3889
9	.3853	.3211	.3056	.3619	.3462

	700-100	700-150	700-200	700-250	700-300
3	.3854	.3571	.3434	.3232	.3300
6	.3153	.3036	.2870	.3009	.3243
9	.3036	.2500	.2174	.2321	.2804

clearly that no single interval combination is significantly better than any other combination. Overall, any of the 1000 or 850 level combinations produced roughly the same statistical results. The surface combinations appear to be very good in the first three or four hours, but rapidly deteriorate as they fail to move the surface feature fast enough. The 700 mb combinations move the area too quickly and too far north. All combinations have the problem that the main area of temperature advection does not move far enough south during the nine hour period. Two factors explain these deficiencies. One is that the low level winds at Huron and Rapid City, South Dakota have virtually no northerly component at 1200 GMT as the front is passing the stations at the time of observations. Second is the eastward movement of the trough through the upper part of the United States during the day which serves to strengthen the northerly flow.

The second criterion is based on a visual comparison of the actual and forecast grids. Since the cold advection area was moving rapidly southeastward during the day, the intensity and area of the cold advection increases dramatically over the 9 hour period. A centerline was chosen for both the predicted and verification fields of strongest cold advection. Visual inspection of forecast and verifying centerlines indicate that the 850 combinations did slightly better than the 1000 mb and 700 mb combinations, and much better than the surface combinations by 9 hours.

Additional insight on the computed steering wind is obtained by analysis of the normalized density-weighted wind field itself. Figure 9 presents three fields for April 5, 1979 case; 850-300 mb, 850-200 mb, and 700-300 mb. The layer wind fields show the flow to be cyclonic with the large scale trough with a distinct maximum at or just behind the secondary front in North Dakota.

The 700-300 mb layer winds (Figure 9A) possess a greater wind maximum and this leads to the faster movement of the front. The 850 mb-based layers are quite similar indicating the addition of 250 mb and 200 mb data into the layer average does little to change the resultant field. Note the verification scores from the 850-200 mb and 850-300 mb forecasts are nearly identical.

The use of the third version of this advection program, ADVECT-2, to produce a time series of forecast values of the critical parameter from the advection model is presented in Figure 10. Forecast and observed advection values for the grid point nearest three cities downstream from the strong front are displayed. The forecast data is excellent for Minneapolis indicating a distinct maximum in the surface temperature advection field between forecast hours 5 and 7. The observed trend shows the maximum temperature advection did peak at the forecast time; however, the advection pattern is stronger than forecast due to the strengthening of the temperature gradient caused by diurnal heating ahead of the front during the day. The forecast trend of the frontal advective field is very useful in this case for indicating to the forecaster the time of frontal passage and maximum frontal activity. Similar plots for two other stations, Sioux Falls and Des Moines, downstream of the secondary front are presented on panels B and C. For these stations the trend of the forecast is also useful, particularly in the timing of the event. However, the observed temperature advection is stronger as with the case of the Minneapolis forecast.

3.4 January 10-11, 1980.

The focus of the second case for testing the advection algorithm was a strong cold front that moved rapidly southeastward through the northern third of the United States during January 11, 1980. The cold front was coupled with

an intense low pressure system that moved northeastward through northern Minnesota and Lake Superior and was characterized by a very sharp temperature gradient and high winds. The central pressure of the low dropped from 985 mb at 0300 GMT (January 11) to 968 mb at 0000 GMT of the 12th. It then slowly weakened and drifted off to the northeast. The cold front was most intense at 1200 GMT of the 11th as it passed through Wisconsin. The front was weakening rapidly by 2100 GMT of the 11th.

The upper air pattern was dominated by a deep trough located near the West Coast. The short wave associated with the surface low moved eastward from this trough and through a weak ridge over the Midwest by 0000 GMT of the 11th, and began to occlude at 1200 GMT of the 12th north of Minnesota. A 120 knot jet streak was associated with the short wave at 300 mb at 1200 GMT on the 12th.

The data base for the January case consisted of two periods. One test used the 0000 GMT upper air data, and the second used the 1200 GMT data. During the 0000 GMT period, the 500 mb trough was just entering the western plains. The surface low pressure system, in response to the upper air pattern, was moving out into the plains and the cold front was starting to plunge southward. During the 1200 GMT period, the 500 mb trough was positioned over northern Minnesota and had occluded. The surface low had deepened and was positioned just north of Lake Superior as the cold front was rapidly moving through Wisconsin at this time. The results will be summarized separately for the two time periods.

3.4.1 0000 GMT 11 January results. The results of application of the advective algorithm to 0000 GMT 11 January are presented in Figure 11 and Table 8. The layer 850-200 mb mean wind is shown in Figure 12. The three hour forecast

was excellent indicating movement of the frontal zone into the central Dakotas and western Nebraska. Deficiencies appear by the 6 hour mark as the forecast is too slow. The observed front bows outward by 0600 GMT 11 January reaching eastern Nebraska while the forecast frontal axis lags to the west. The forecast frontal position on the northern or southern ends are considerably better. By nine hours the forecast axis trails the observed front by 200 km. The basic weakness of the forecast was the absence of a distinct momentum core core in the mean layer winds (Figure 12) which would have moved the central region of the front faster. The use of model data in the advective algorithm would be required to capture the development of the momentum core after the 3 hour mark to improve the prediction. The threat scores, Table 8, describe the poorer performance of the advection forecasts for hours 6 and 9. Due to the stronger advection area standard deviations of 1.5 (approximately 20°C/day) was used to delineate the frontal area and compute the statistical scores. Note that there is little difference in forecast skill between the various mean layers. From a visual examination of the forecasts, the layers with bases at 850 mb and 1000 mb do slightly better but the differences are not statistically significant.

3.4.2 1200 GMT 11 January results. The results for data 1200 GMT 11 January is presented in Figure 13 and Table 9. The threat scores are also computed on the frontal area exceeding 20°C/day, 1.5 standard deviation of the field. Comparison of actual and forecast frontal axes and an inspection of the threat scores shows the forecasts to be extremely good through hour 6 and useful even at hour 9. The layer wind SFC-400 mb (shown on Figure 12b) yielded the best statistical scores; however, all combinations did well. Again the layers which include 850 mb and 1000 mb data do better than layers which start at

Table 8

Threat Scores for Advective Forecasts
From 0000 GMT 11 January 1980

	SFC-400	SFC-500	SFC-200	SFC-250	SFC-300
3	.4000	.3200	.4694	.4694	.4375
6	.1169	.1154	.1250	.1392	.1266
9	.0103	.0000	.0412	.0306	.0104

	1000-100	1000-150	1000-200	1000-250	1000-300
3	.5652	.5208	.5532	.5106	.4894
6	.2078	.1948	.1807	.1667	.1688
9	.1505	.1489	.1290	.1146	.1170

	850-100	850-150	850-200	850-250	850-300
3	.5652	.5208	.5532	.5106	.4894
6	.2078	.1948	.1807	.1667	.1688
9	.1505	.1489	.1290	.1146	.1170

	700-100	700-150	700-200	700-250	700-300
3	.5000	.5306	.5098	.4898	.5319
6	.2000	.2222	.1786	.1875	.1585
9	.1720	.1809	.1443	.1429	.1340

Table 9

Threat Scores for Advective Forecasts
From 1200 GMT 11 January 1980

	SFC-400	SFC-500	SFC-200	SFC-250	SFC-300
3	.7164	.6000	.7286	.7324	.7206
6	.5775	.5405	.4270	.4699	.5250
9	.3293	.3816	.2268	.2553	.3023

	1000-100	1000-150	1000-200	1000-250	1000-300
3	.6173	.6173	.6375	.7027	.7324
6	.3301	.3173	.3173	.3936	.4494
9	.1239	.1239	.1111	.1130	.1604

	850-100	850-150	850-200	850-250	850-300
3	.6173	.6173	.6456	.7027	.7183
6	.3301	.3143	.3367	.3895	.4494
9	.1239	.1140	.1111	.1130	.1495

	700-100	700-150	700-200	700-250	700-300
3	.5632	.5568	.5632	.5814	.6220
6	.2521	.2542	.2710	.3238	.3700
9	.0859	.0859	.0846	.0873	.0826

700 mb.

3.5 Conclusions.

The results of these test cases are encouraging. These preliminary results illustrate the potential of a simple algorithm to provide short-range guidance of frontal weather using an interactive computer system which can access a variety of meteorological data.

4. SUMMARY

This year's work focused on the statistical determination of adverse weather regions and the advection of surface and frontal features using an interactive computer system. The goal of the statistical study was the objective determination of thunderstorm occurrence and severity from satellite derived statistics. Collocated surface hourly data and satellite data were obtained using a semi-automated data acquisition procedure using McIDAS. Thirty-four hours of data were collected between 18 April 1980 and 7 June 1980 comprising 5570 station reports of which 2.7% reported thunderstorms. Discriminant analysis routines performed on the data yielded eight statistically significant discriminant models. Model actual accuracy ranged from .729 to .813 . The models emphasized the importance of temporal and multi-spectral predictors in thunderstorm specification.

The second focus of this year's activity is the development of an advective forecast algorithm for short-range prediction of frontal and other surface features. The algorithm uses a Lagrangian advective method with density-weighted mean tropospheric wind computed from mandatory level rawinsonde data. Detailed results from two cases establish that the advective scheme shows considerable skill in forecasting the movement of surface frontal signatures. The study of the various lower and upper limits for the specification of the mean wind indicate only small differences in performance.

ACKNOWLEDGMENTS

The authors express their appreciation to John R. Stremikis for assistance in figure preparation and editing, Marty Barrett for McIDAS programming assistance, Nancy Malz and Jean Johnson for typing various drafts of this report and the final manuscript.

BIBLIOGRAPHY

Adler, R. F., and D. D. Fenn, 1979a: Satellite-based thunderstorm intensity parameters. J. Appl. Meteor., 18, 502-517.

Adler, R. F., and D. D. Fenn, 1979b: Thunderstorm vertical velocities estimated from satellite data. J. Atmos. Sci., 36, 1747-1754.

Anderson, R. K., E. W. Ferguson, and V. J. Oliver, 1966: The use of satellite pictures in weather analysis and forecasting. World Meteorological Organization Technical Note No. 75, WMO-NO. 190, 96 pp.

Anderson, R. K., J. P. Ashman, F. Bittner, G. R. Farr, E. W. Ferguson, V. J. Oliver, and A. H. Smith, 1969: Application of meteorological satellite data in analysis and forecasting. ESSA Technical Report NESC 51, U. S. Department of Commerce, 185 pp.

Chatters, G. C., and V. E. Suomi, 1975: The applications of McIDAS. IEEE Trans. Geosci. Electron., GE-13, 137-146.

Conover, J. H., 1962: Cloud interpretation from satellite altitudes. Res. Note 81, Air Force Cambridge Research Laboratories, 55 pp.

_____,1963: Cloud interpretation from satellite altitudes. Res. Note 81, Suppl. 1, Air Force Cambridge Research Labs, 18 pp.

Cooley, W. W., and P. R. Lohnes, 1971: Multivariate Data Analysis. John Wiley and Sons, Inc., 364 pp.

Darling, E. M., and R. D. Joseph, 1968: Pattern recognition from satellite altitudes. IEEE Trans. Syst. Sci. Cybern., SSC-4, 38-47.

Donaldson, R. J., R. M. Dyer, and M. J. Kraus, 1975: An objective evaluator of techniques for predicting severe weather events. Preprints Ninth Conf. Severe Local Storms, Amer. Meteor. Soc., Norman, 321-326.

Erickson, C. O., and L. F. Hubert, 1961: Identification of cloud forms from TIROS I pictures. Meteorological Satellite Laboratory Report-7, U.S. Dept. of Commerce, pp.

Fye, F. K., 1978: The AFGWC automated cloud analysis model. AFGWC Technical Memorandum 78-002, Air Force Global Weather Central, 97 pp.

Glahn, H. R., D. A. Lowrey, and G. W. Hollenbaugh, 1969: An operational subsynoptic advection model. ESSA, Weather Bureau Tech. Memo WBTM-23, July, 1969.

Harris, R., and E. C. Barrett, 1975: An improved satellite nephanalysis. Meteor. Mag., 104, 9-16.

_____, and _____, 1978: Toward an objective nephanalysis. J. Appl. Meteor., 17, 1258-1266.

Keegan, T. J., 1978: Variation in groud brightness over the northeastern United States as sensed by GOES satellites. AFGL-TR-78-0290, 20 pp.

Lachenbruch, P. A., 1975: Discriminant Analysis. Hafner Press, 128 pp.

Madison Academic Computing Center, 1978: Random Number Routines. Reference Manual, University of Wisconsin-Madison, 79 pp.

Mosher, F. R., 1973: Cloud brightness contrasts as viewed by a satellite. M.S. Thesis, University of Wisconsin-Madison, 60 pp.

Muench, H. S., and T. J. Keegan, 1978: Automated short-range forecasting of cloud cover and precipitation using geo-synchronous satellite imagery data. Preprints Eighth Technical Exchange Conf., Colorado Springs, 113-117.

Negri, A. J., D. W. Reynolds, and R. A. Maddox, 1976: Measurements of cumulunimbus clouds using quantitative satellite and radar data. Preprint Volume of Seventh Conference on Aerospace and Aeronautical Meteorology, Melbourne, 119-124.

Neter, J., and W. Wasserman, 1974: Applied Linear Statistical Models. Richard D. Irwin, Inc., 842 pp.

Riggio, R. F., and K. L. Topham, 1979: Using discriminant analysis to predict rainshower occurrence in the Texas HIPLEX area. Preprints Sixth Conf. on Prob. and Stat. in Atmos. Sci., Banff, 74-78.

Schlater, J., and J. Learn, 1975: DISCRIM1: Discriminant Analysis. Academic Computing Center, University of Wisconsin-Madison, 55 pp.

Sikdar, D. N., and V. E. Suomi, 1972: On the remote sensing of mesoscale tropical convection intensity from a geostationary satellite. J. Appl. Meteor., 11, 37-43.

Sikula, G. J., and T. H. Vonder Harr, 1972: Very short range local area weather forecasting using measurements from geosynchronous meteorological satellites. Colorado State Univ. Atmospheric Science Paper No. 185, Air Force Contract No. F19628-71-C-0073, 73 pp.

Smith, E. A., 1975: The McIDAS system. IEEE Trans. Geosci. Electron., GE-13, 123-136.

Wash, C. H., and T. M. Whittaker, 1980: Subsynoptic Analysis and Forecasting with an Interactive Computer System. Accepted for publication in Bulletin of the AMS.

Wash, C. H., T. M. Whittaker, and D. R. Johnson, 1979: Initial Studies in objective forecasting of mesoscale weather using interactive computer system. Scientific Report No 1, Air Force Geophysics Laboratory, 18 pp.

Zak, J. A., 1977: Forecasting thunderstorms over a 2- to 5-h period by statistical methods. NASA Contractor Report 2934, 112 pp.

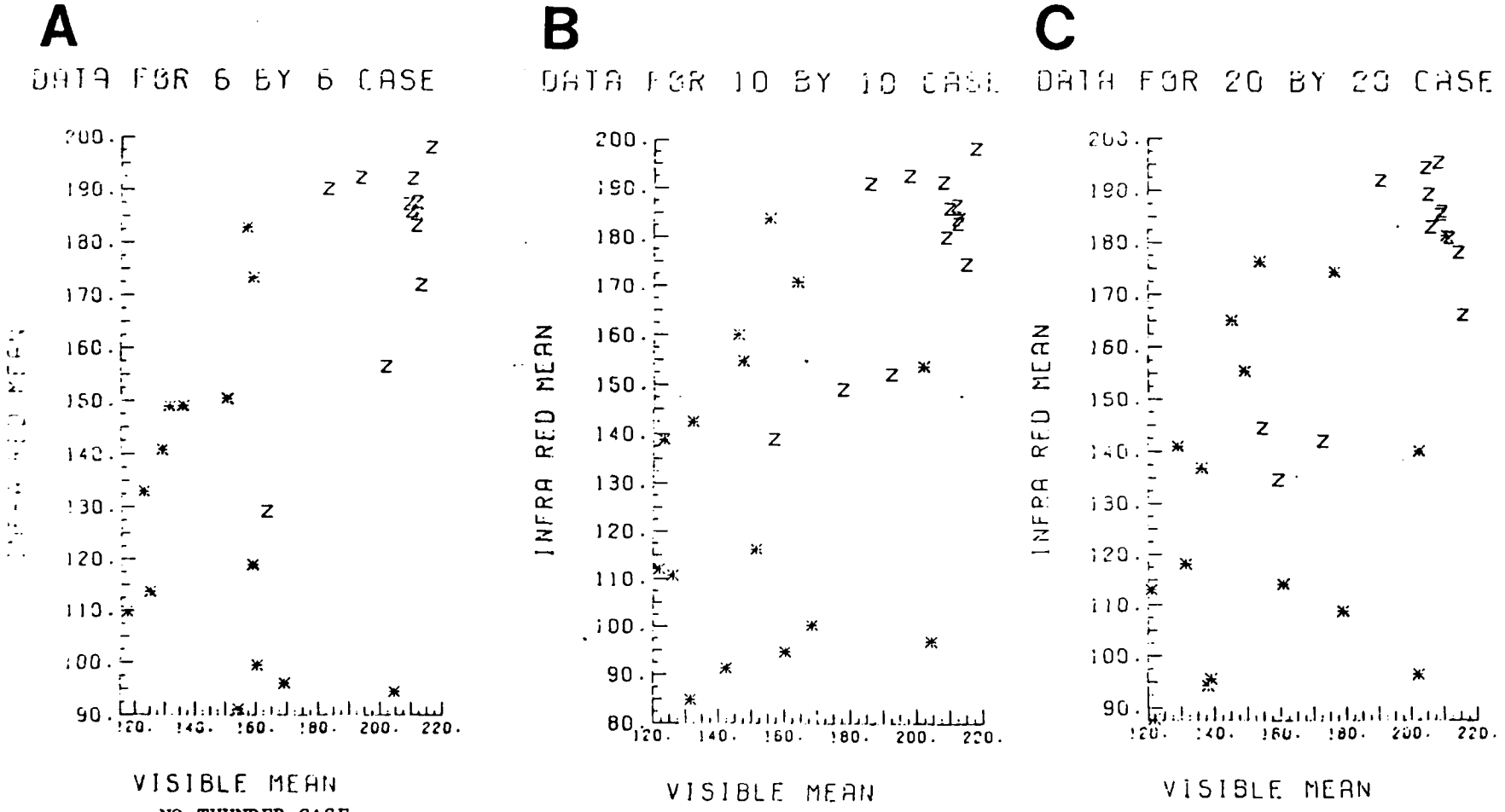

Fig. 1A. Data plot to determine the optimum pixel matrix for data collection--6X6 case.

Fig. 1B. Same as fig. 1A except for 10X10 pixel matrix.

Fig. 1C. Same as fig. 1A except for 20X20 pixel matrix

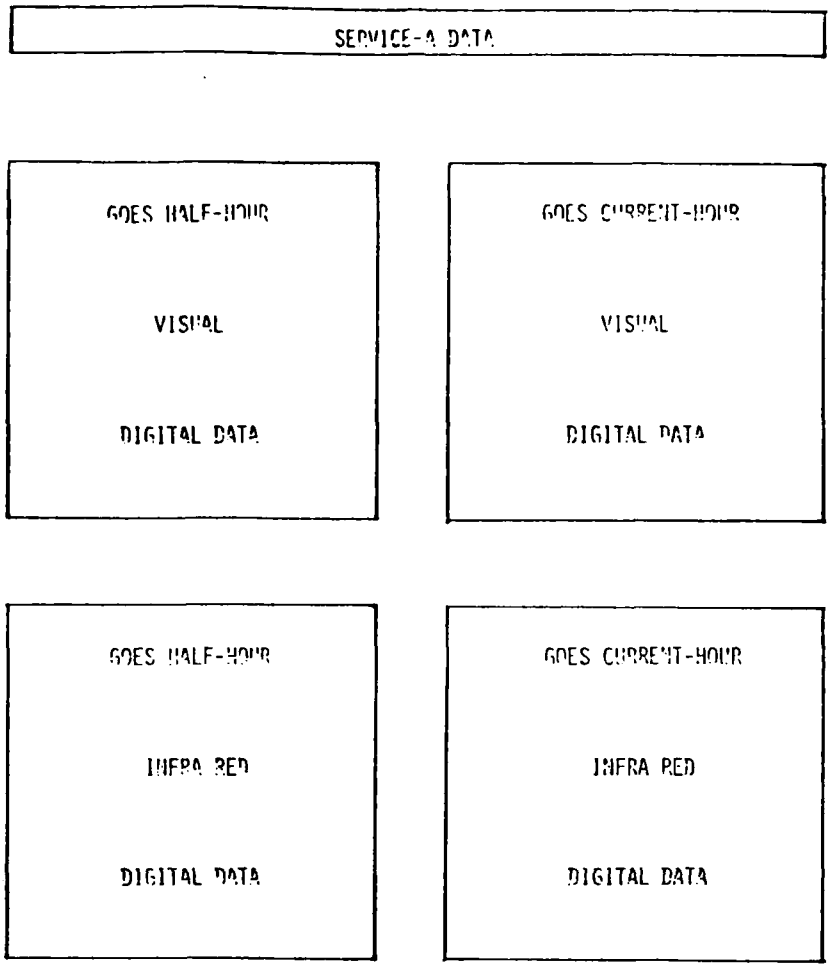

Fig. 2. Schematic diagram of data storage in McIDAS.

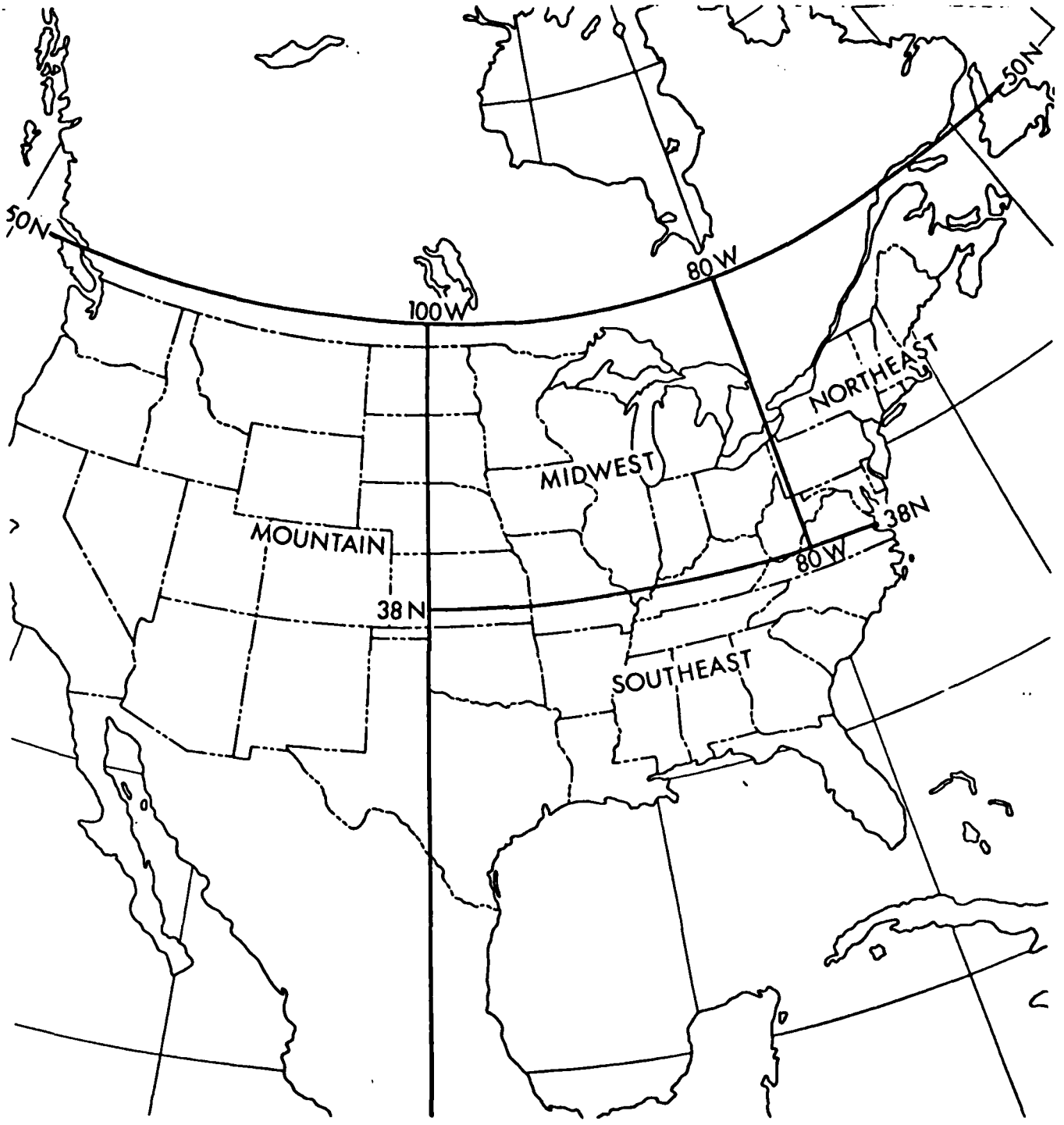

Figure 3. Boundaries for geographical stratification.

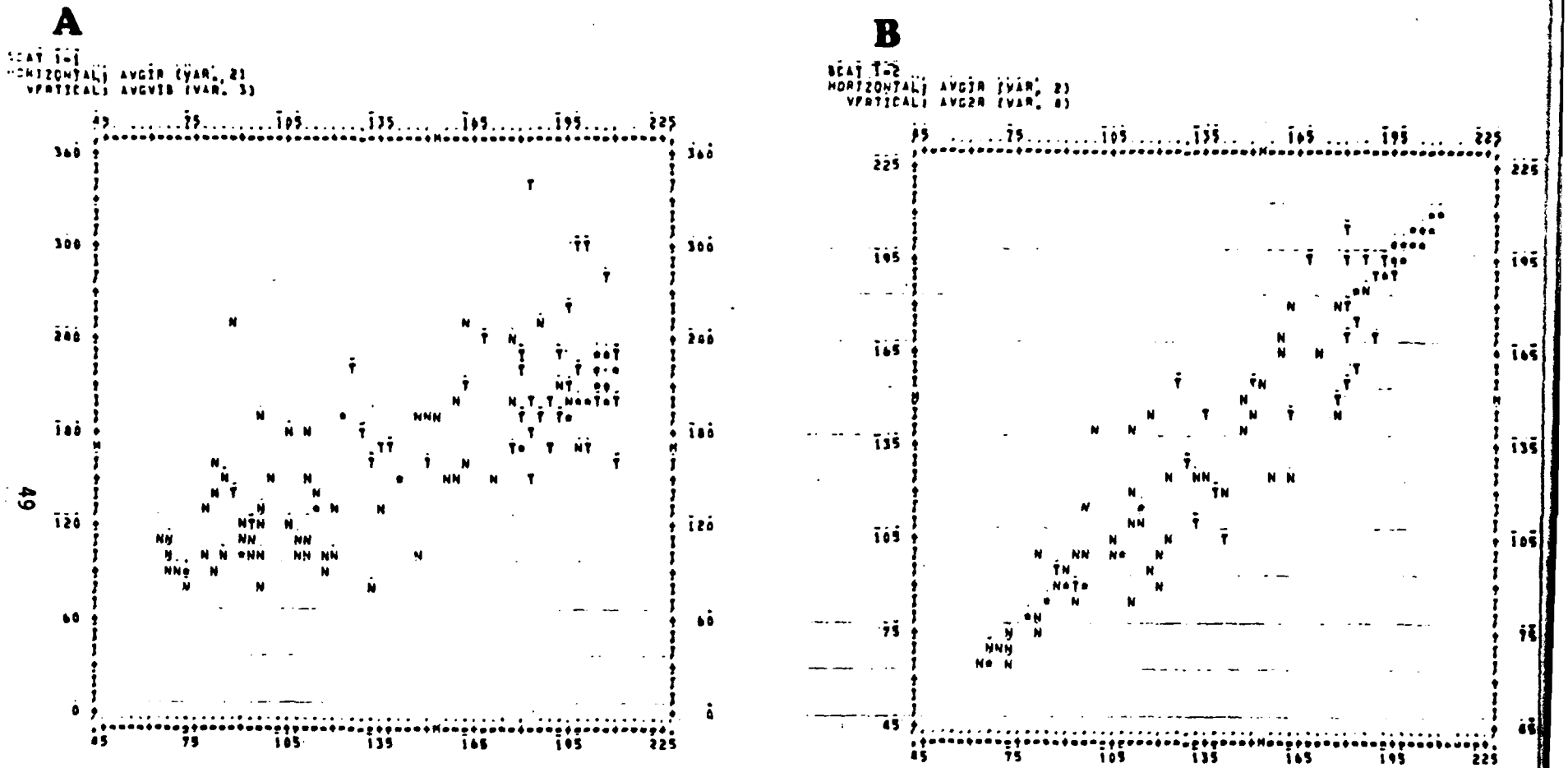

Figs. 4A-40. Plots of thunderstorm and no thunderstorm data for the 15 models investigated. The variables for each model are shown in the upper left hand corner of each plot.

C

SCAT IC)
HORIZONTAL: AVGIR (VAR. 2)
VERTICAL: AVG2V (VAR. 5)

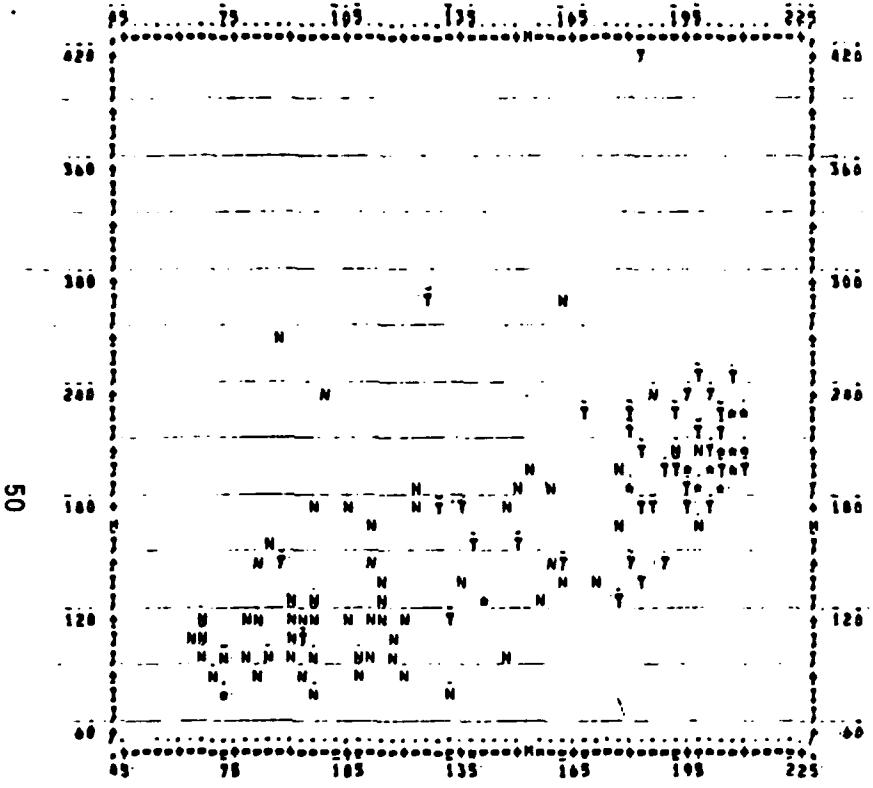

D

SCAT IC)
HORIZONTAL: AVGIR (VAR. 2)
VERTICAL: AVG2R (VAR. 6)

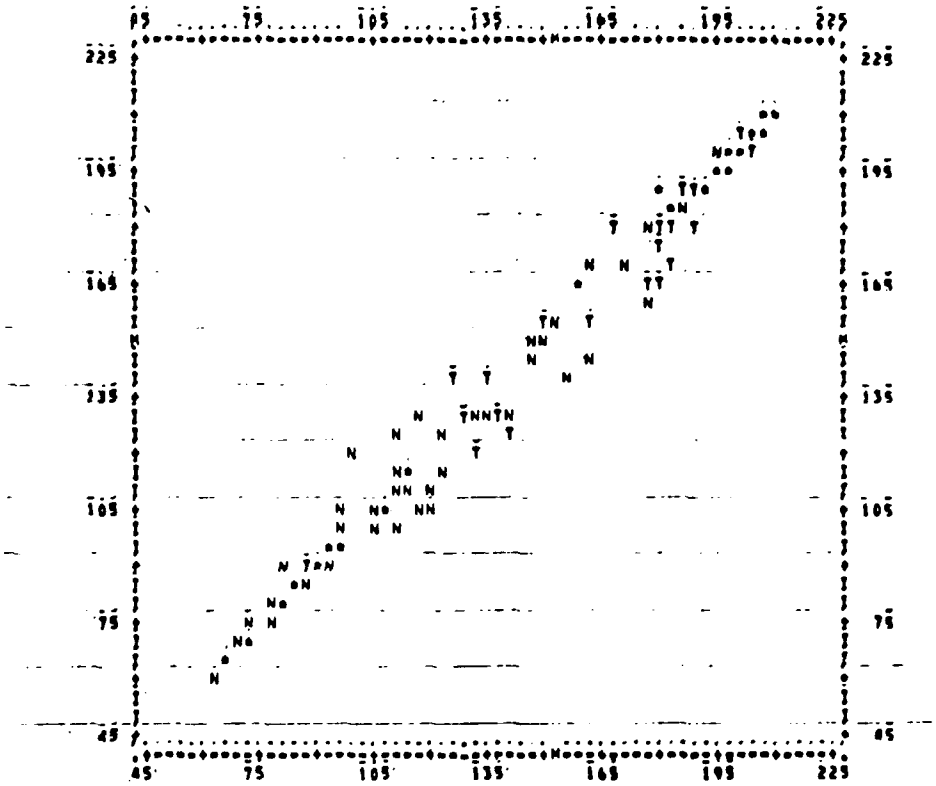

E

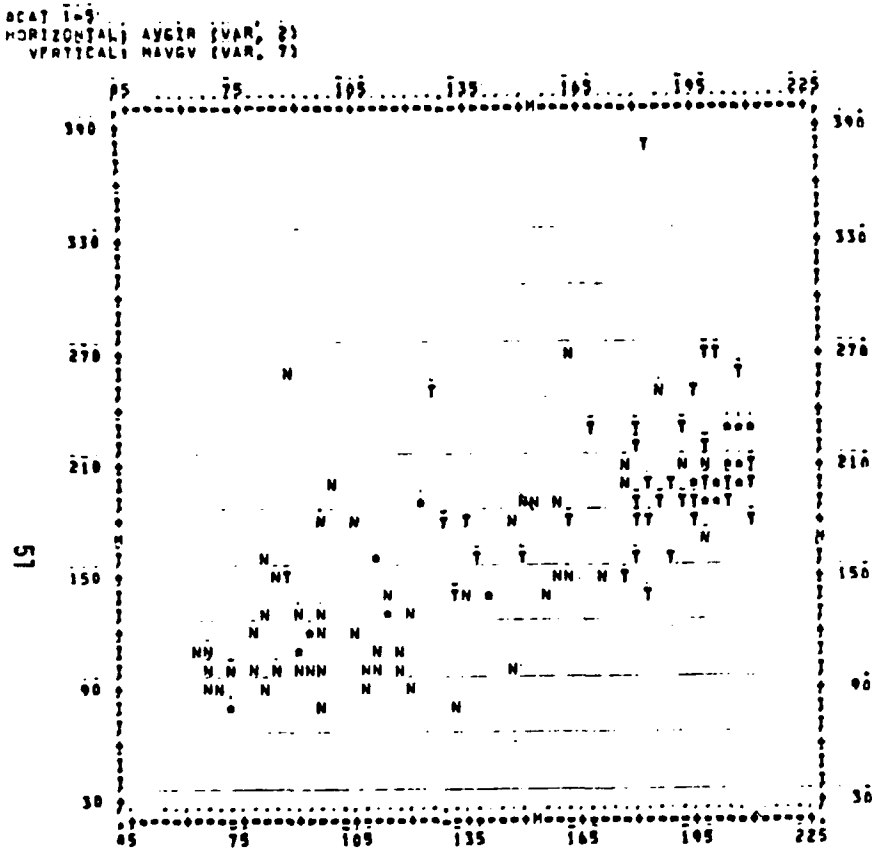
SCAT T=9
HORIZONTAL: AVGIR (VAR. 2)
VERTICAL: NAVGV (VAR. 7)
45
75
105
135
165
195
225
30
90
150
210
270
330
390

F

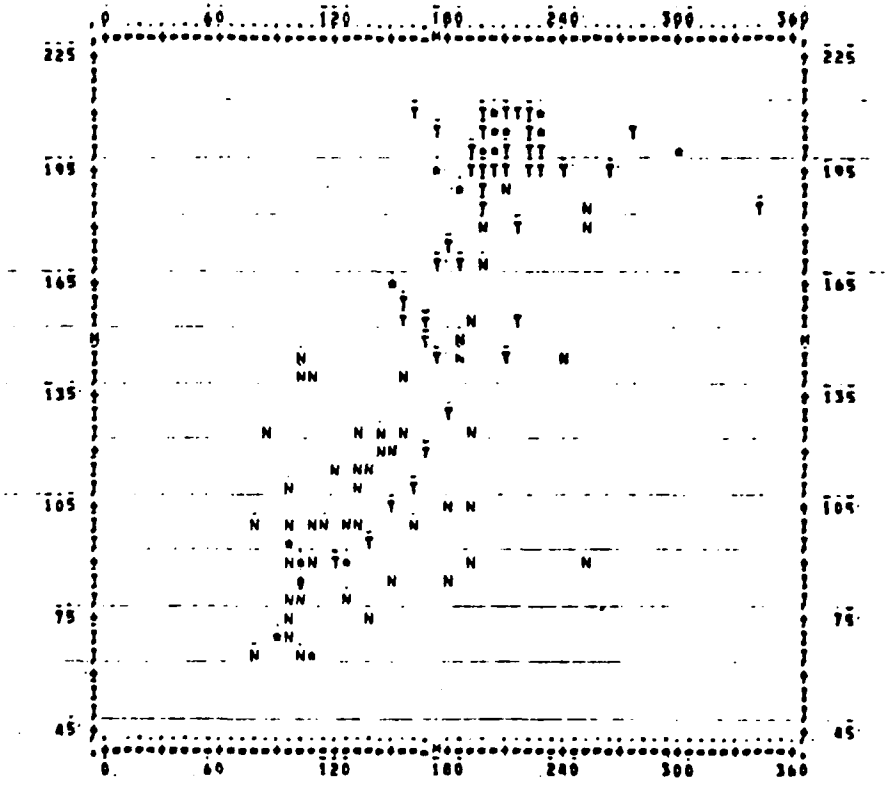
SCAT T=6
HORIZONTAL: AVGVIR (VAR. 5)
VERTICAL: AVG2R (VAR. 6)
0
60
120
180
240
300
360
45
75
105
135
165
195
225

G

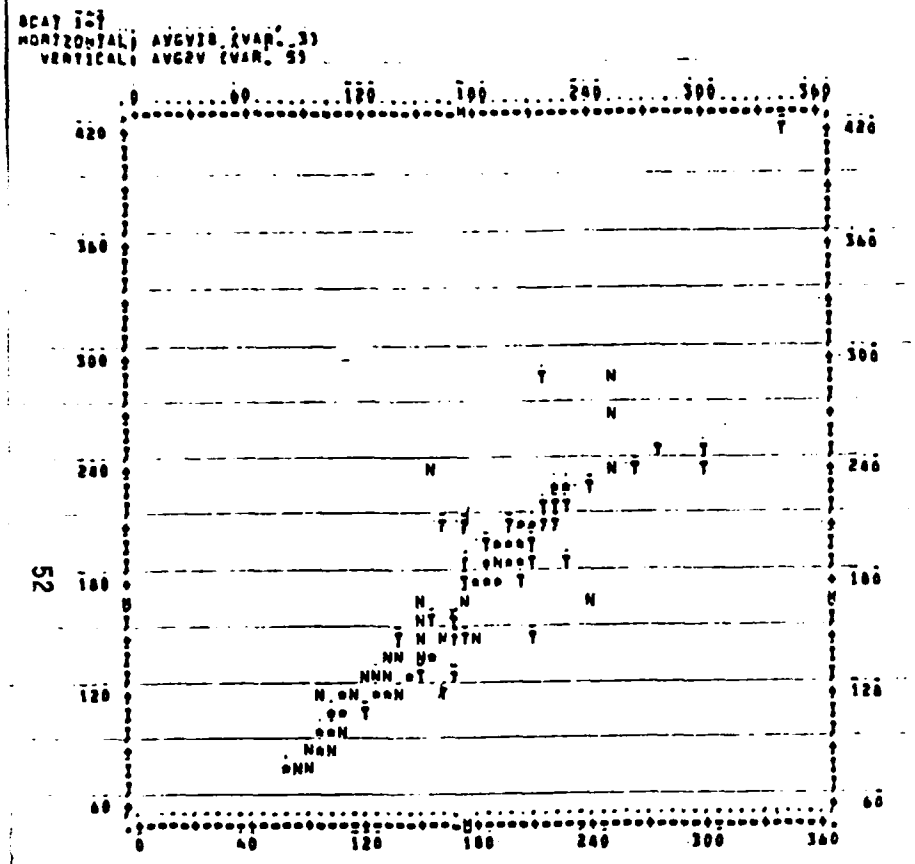
SCAT 101
HORIZONTAL: AVGVIS (VAR. 33)
VERTICAL: AVGRV (VAR. 55)
0
60
120
180
240
300
360
420
360
300
240
180
120
60
0
40
120
180
240
300
360

H

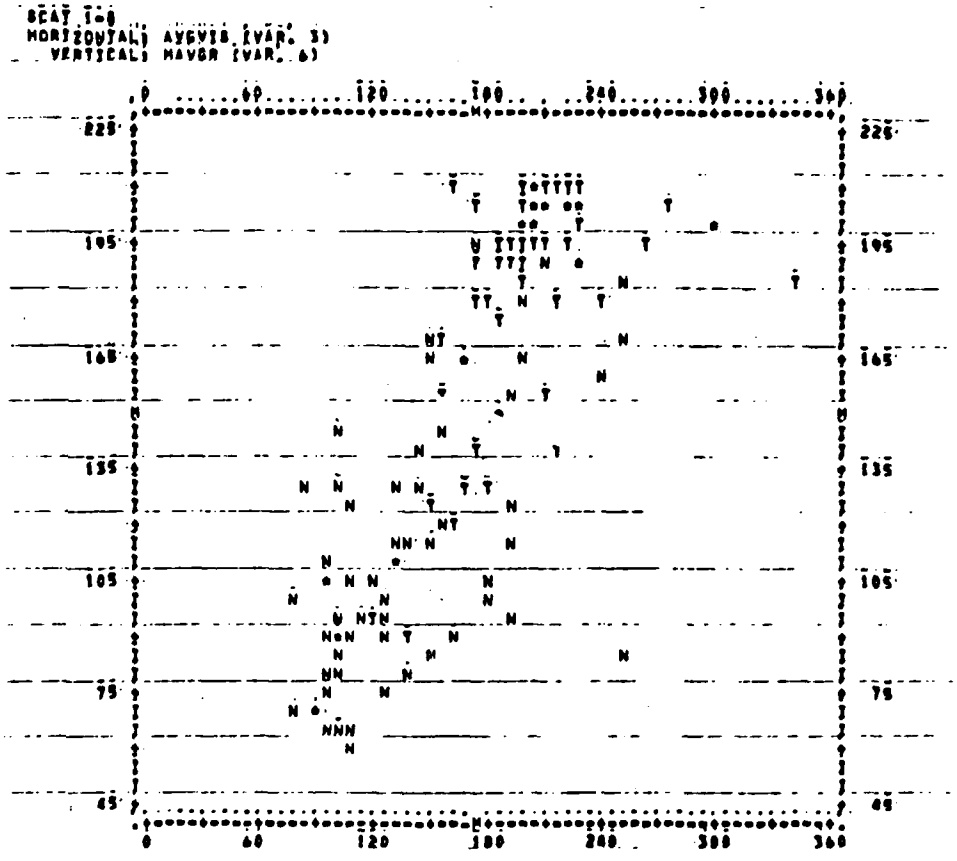
SCAT 108
HORIZONTAL: AVGVIS (VAR. 33)
VERTICAL: MAXGR (VAR. 61)
0
60
120
180
240
300
360
225
195
165
135
105
75
45
0
60
120
180
240
300
360

I

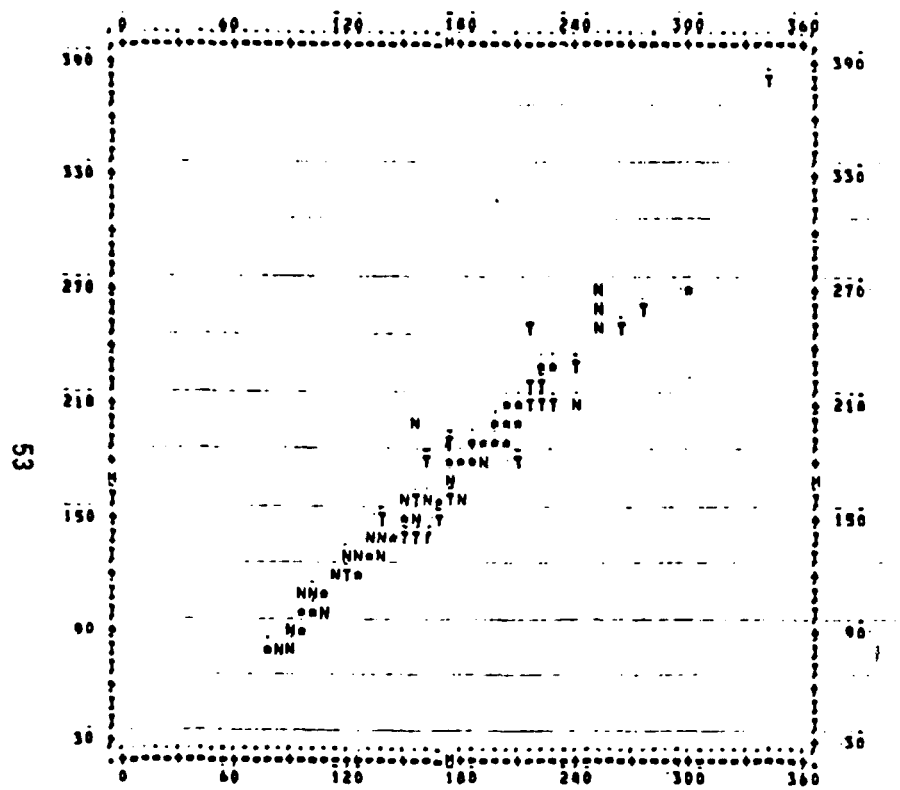
SCAT I=9
HORIZONTAL: AVGV1R (VAR. 3)
VERTICAL: AVGV (VAR. 7)
0
60
120
180
240
300
360
30
90
150
210
270
330
390

J

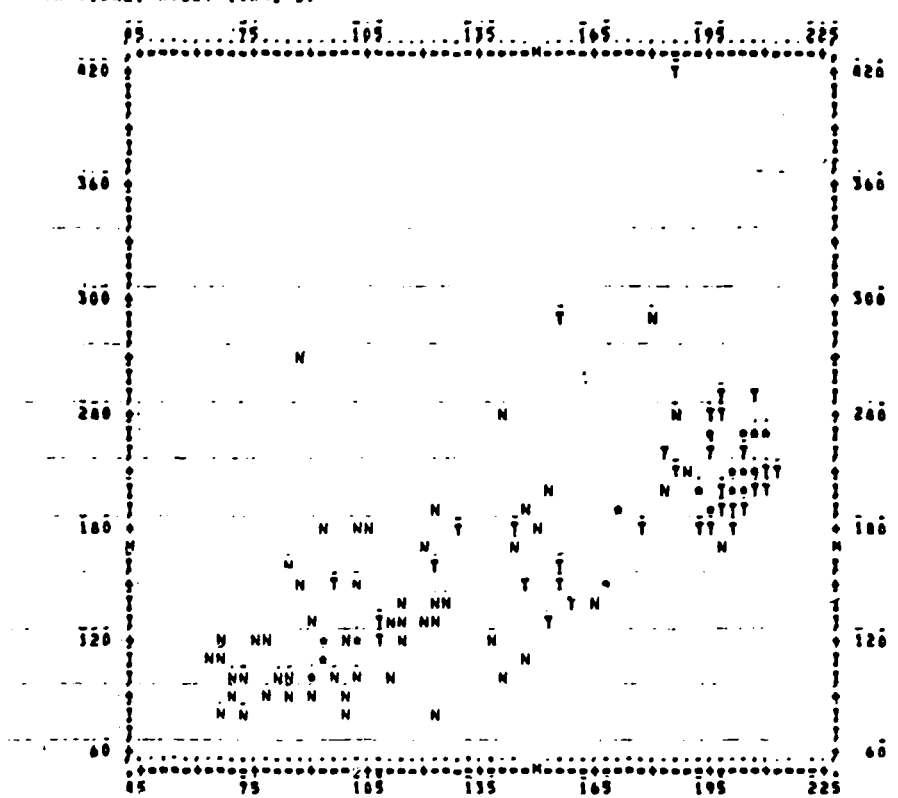
SCAT I=10
HORIZONTAL: AVG2R (VAR. 4)
VERTICAL: AVG2V (VAR. 5)
45
75
105
135
165
195
225
60
120
180
240
300
360
420

K

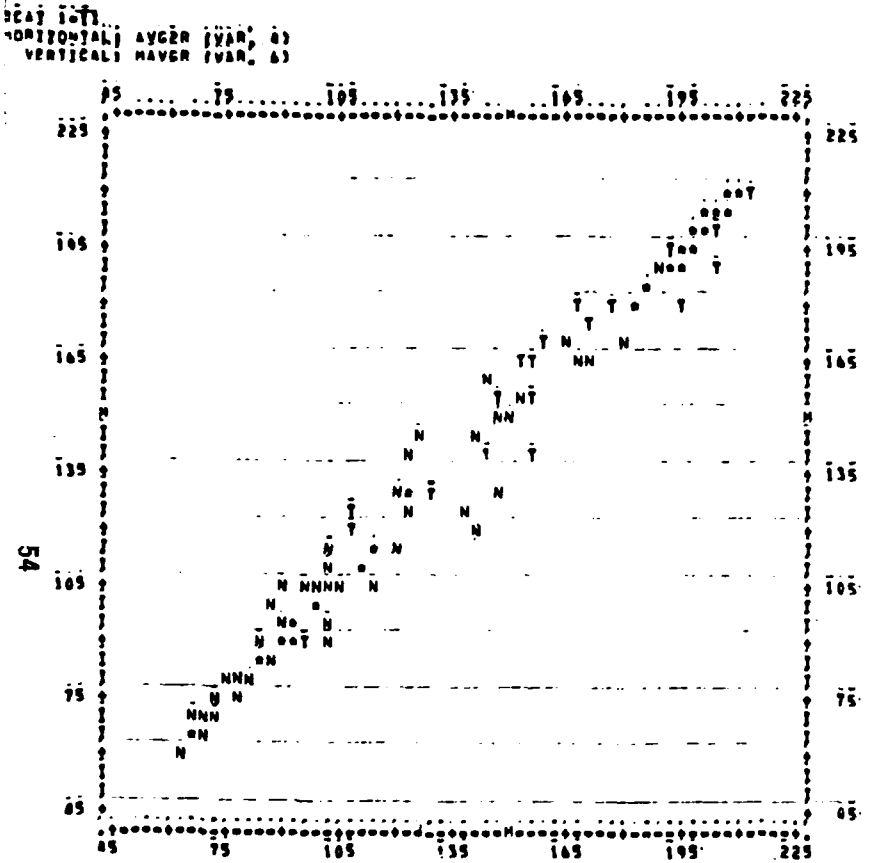
SCAT 1-11
HORIZONTAL: AVGER (VAR, X)
VERTICAL: MAVGR (VAR, X)
45
75
105
135
165
195
225

L

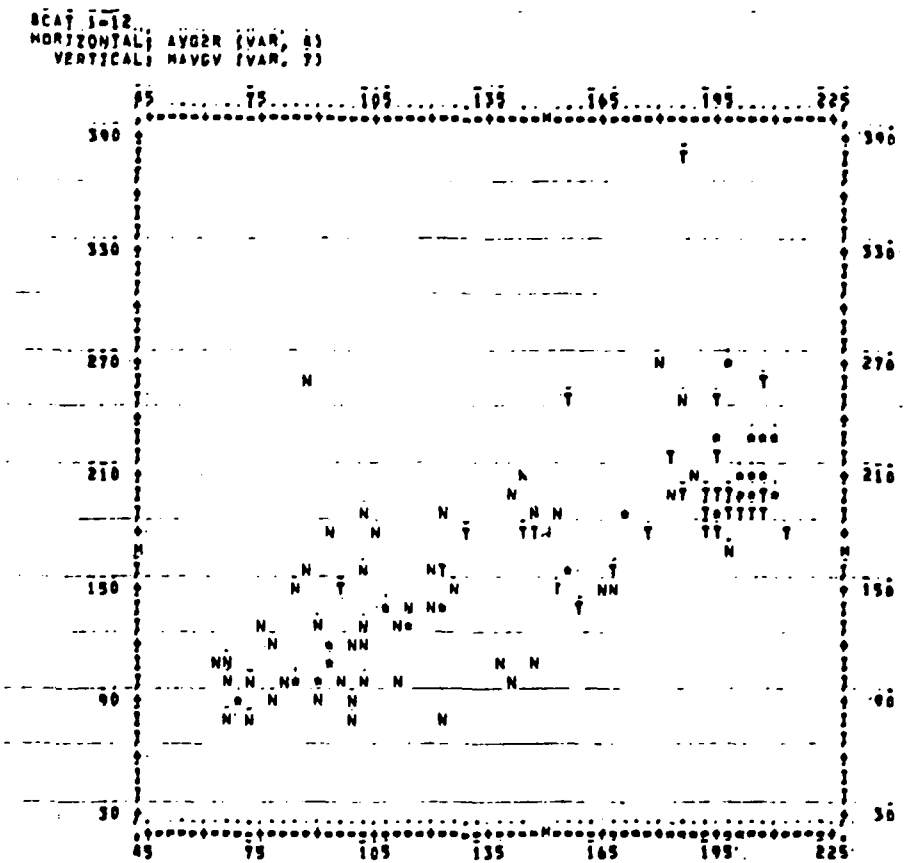
SCAT 1-12
HORIZONTAL: AVGER (VAR, X)
VERTICAL: MAVGV (VAR, Y)
30
90
150
210
270
330
390
45
75
105
135
165
195
225

M

SCAT I=13
HORIZONTAL: AVGZV (VAR, 3)
VERTICAL: MAVGR (VAR, 6)

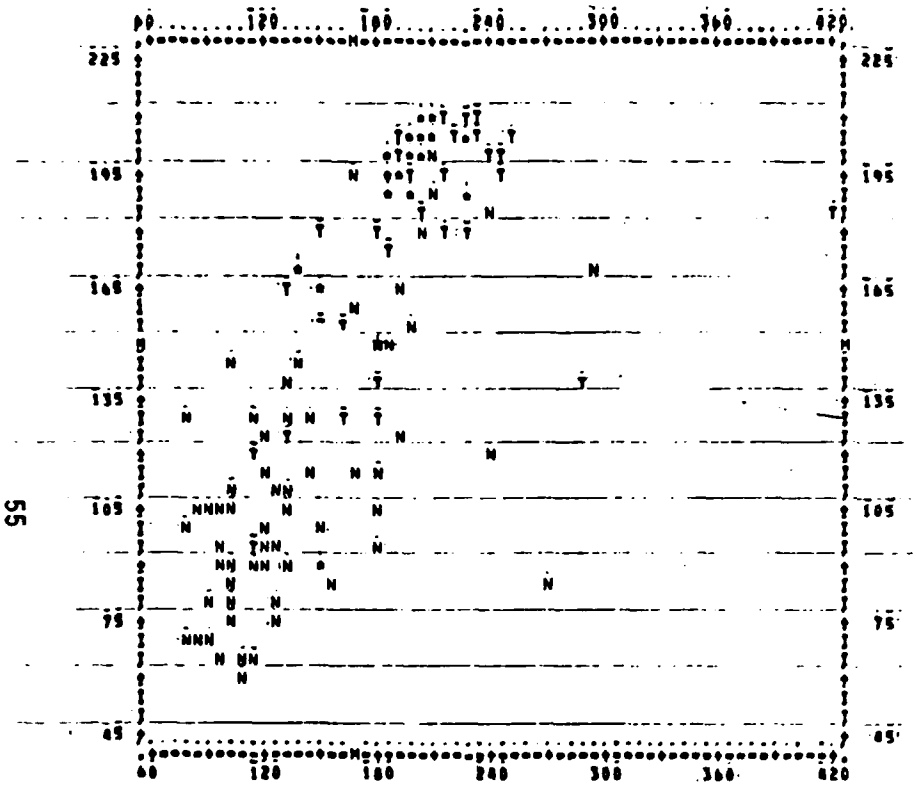

N

SCAT I=13
HORIZONTAL: AVGZV (VAR, 3)
VERTICAL: MAVGV (VAR, 7)

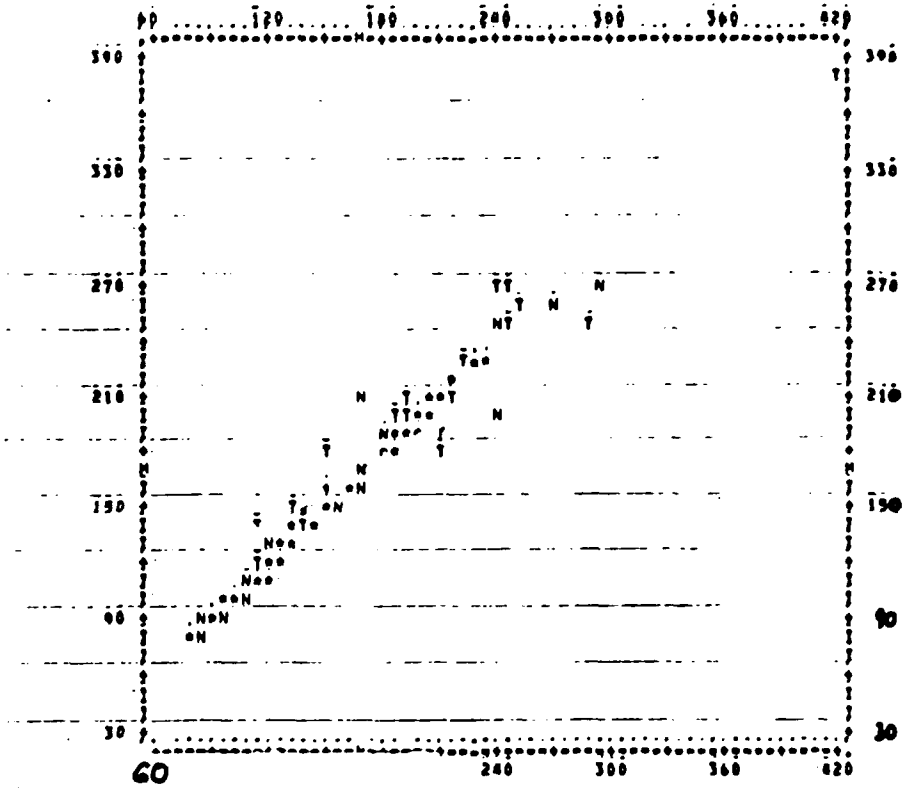

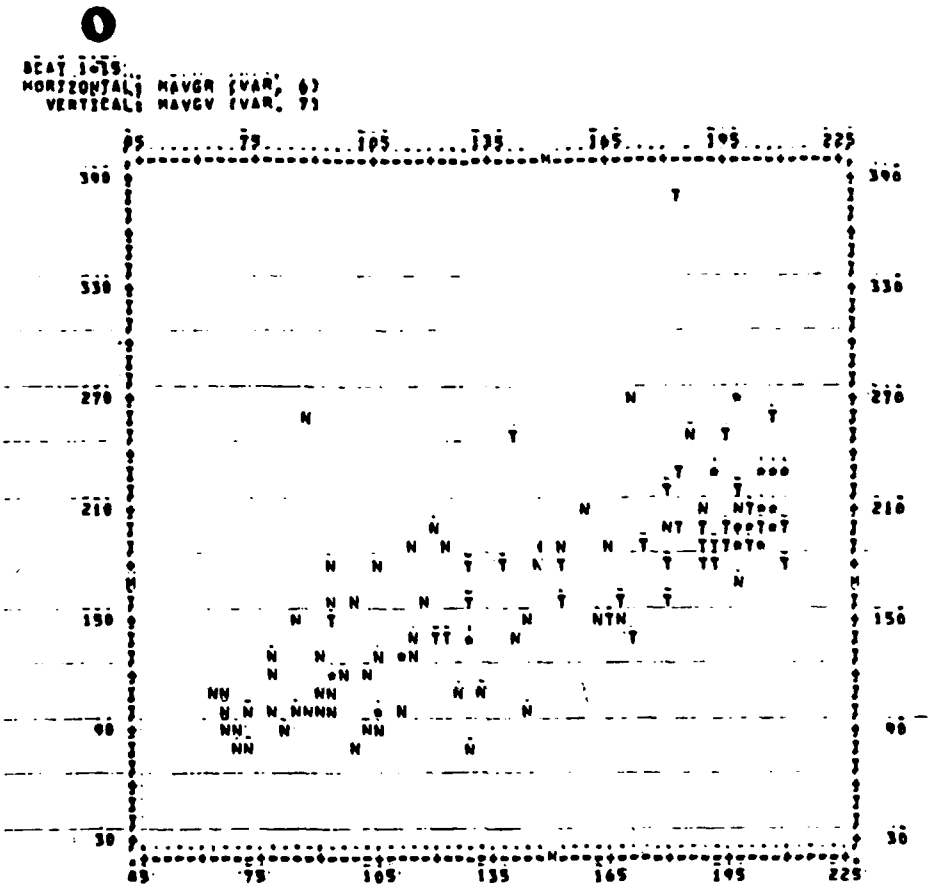
BEAT 1-15
HORIZONTAL: HAVGR (VAR, 6)
VERTICAL: HAVGV (VAR, 7)
45
75
105
135
165
195
225
300
330
270
210
150
90
30

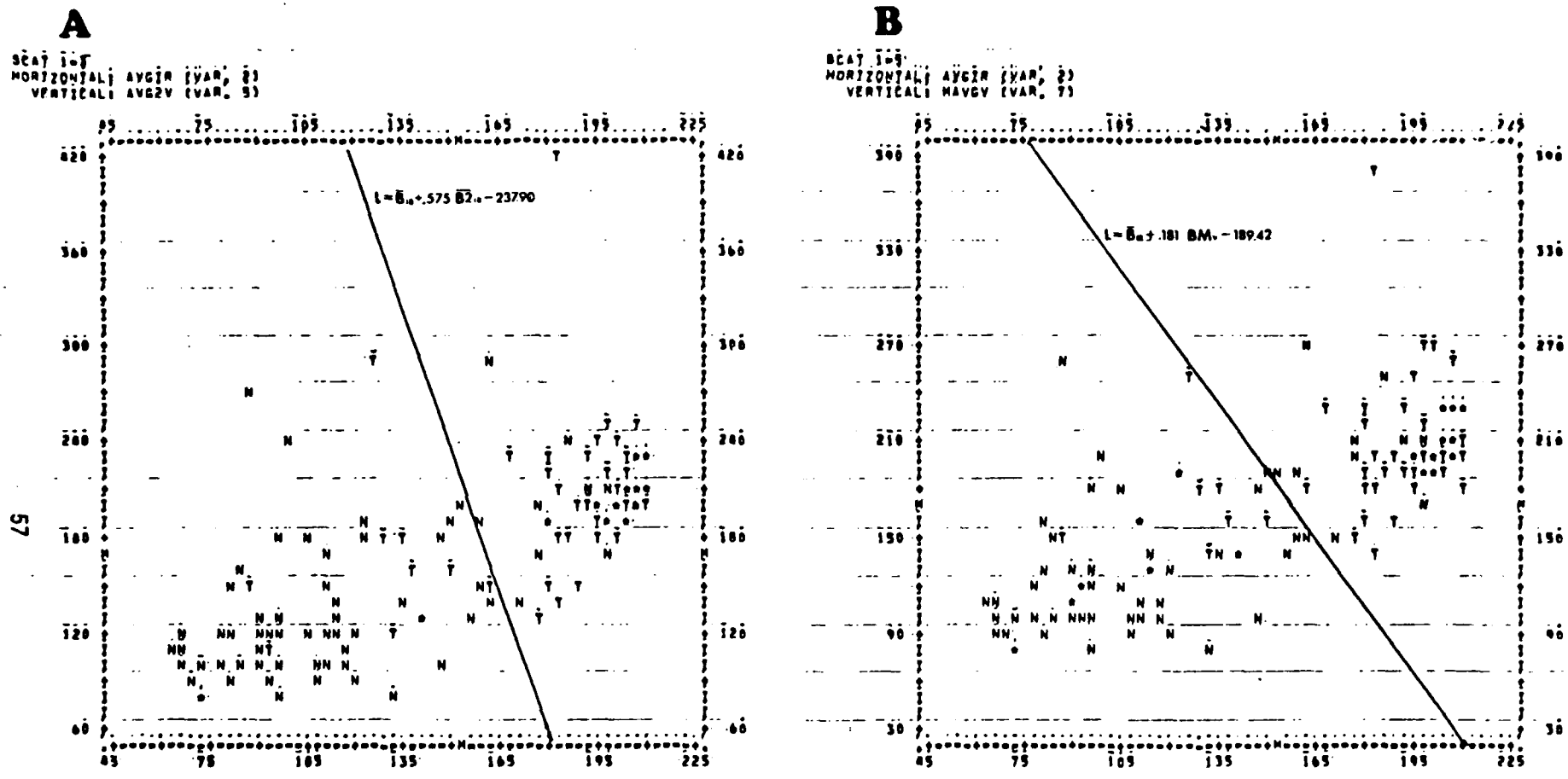

T THUNDERSTROM OBSERVATION

N NO THUNDERSTORM OBSERVATION

* MORE THAN ONE OBSERVATION AT ONE LOCATION

Figs. 5A-5H. Accepted models with plots of data and discriminant functions. The variables for each model are shown in the upper left hand corner of each plot.

C

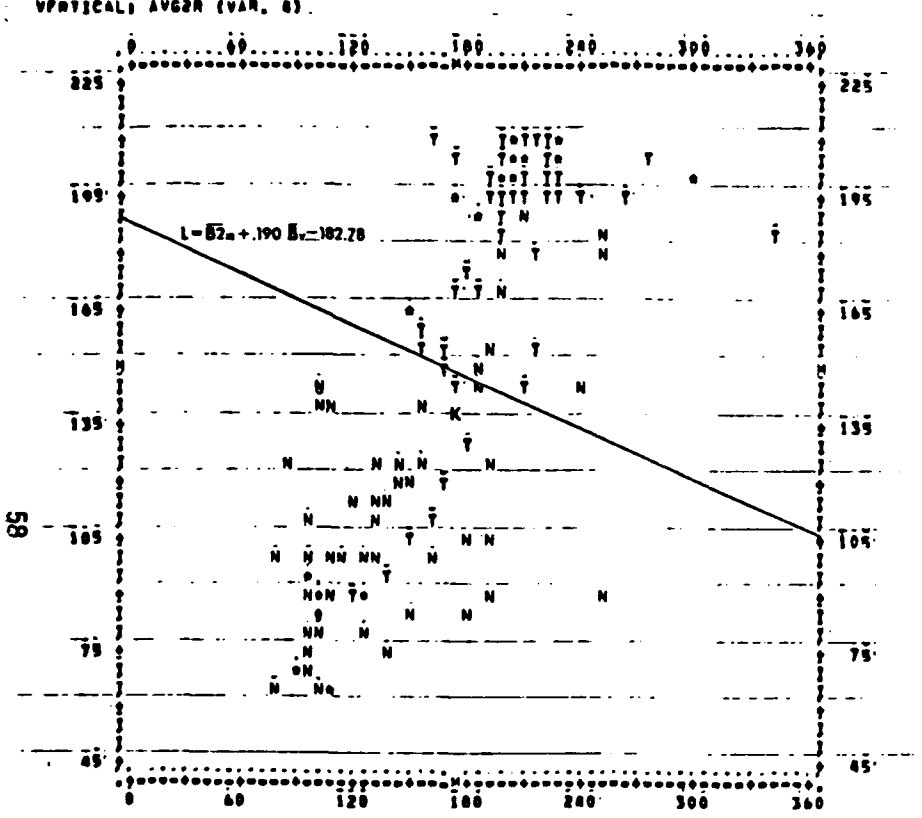
SCAT I=5
HORIZONTAL) AVGVIB (VAR. 5)
VERTICAL) AVG2R (VAR. 6)
L = B̄2m + .190 B̄v = 182.28
0
60
120
180
240
300
360
225
195
165
135
105
75
45

D

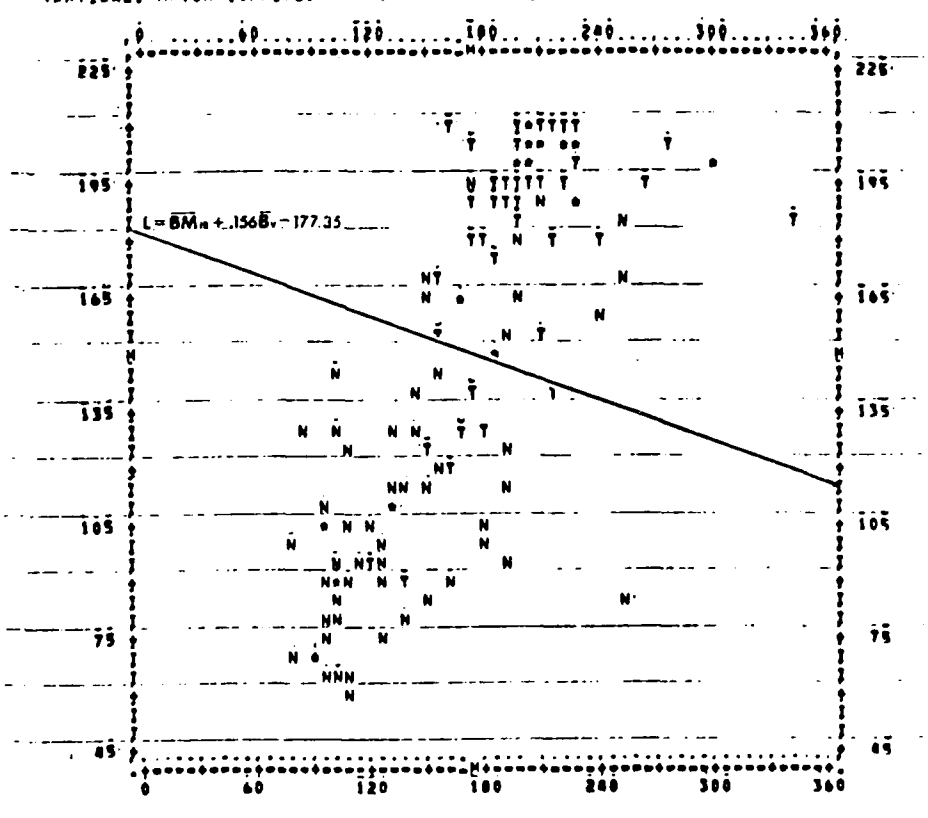
SCAT I=6
HORIZONTAL) AVGVIB (VAR. 5)
VERTICAL) HAVGR (VAR. 6)
L = B̄M2 + .156B̄v - 177.35
0
60
120
180
240
300
360
225
195
165
135
105
75
45

E

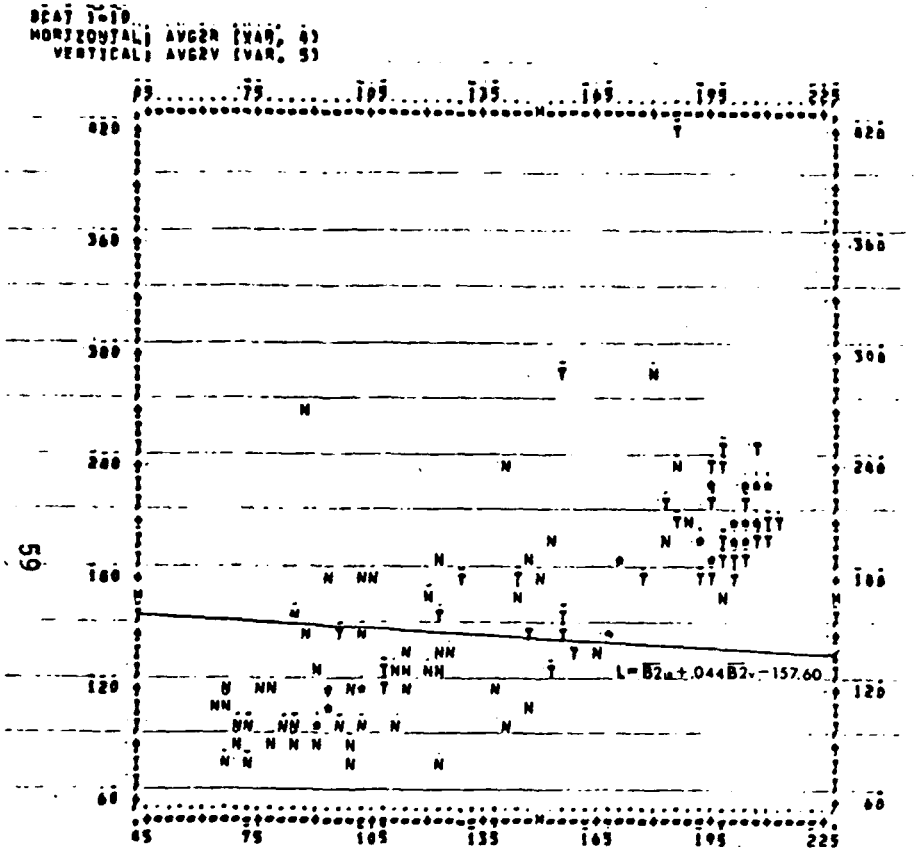
SCAT 1=10
HORIZONTAL: AVG2R (VAR. 4)
VERTICAL: AVG2V (VAR. 5)
L=B2m±.044B2v-157.60

F

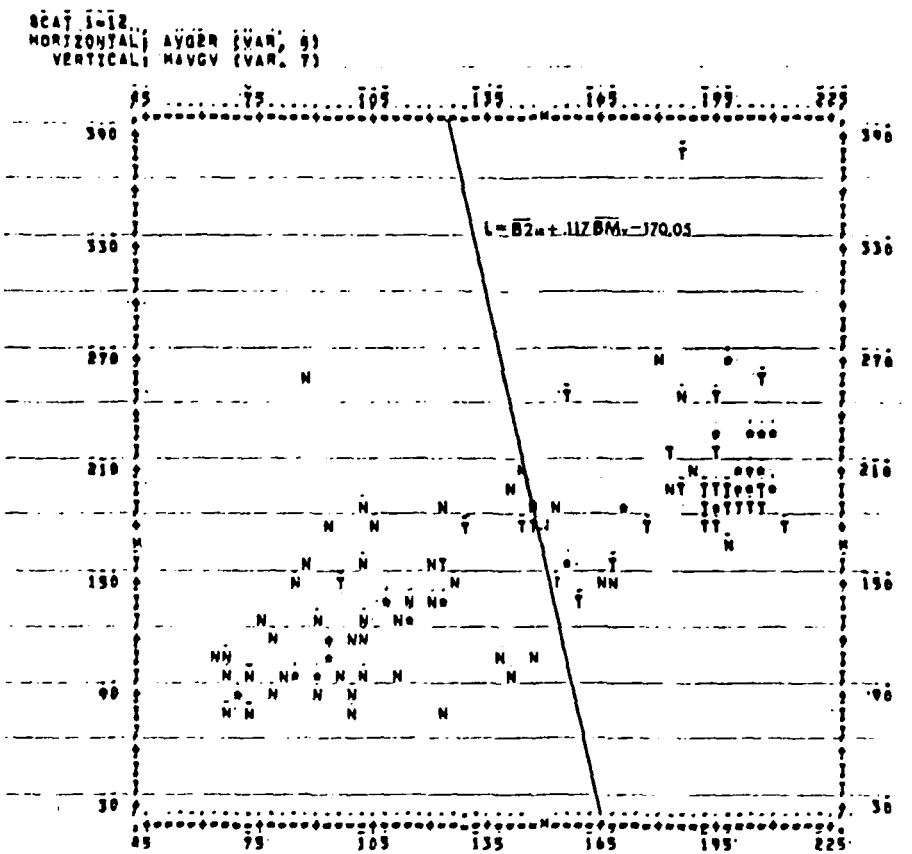
SCAT 1=12
HORIZONTAL: AVG2R (VAR. 4)
VERTICAL: AVGV (VAR. 7)
L=B2m±.112BMx-170.05

G

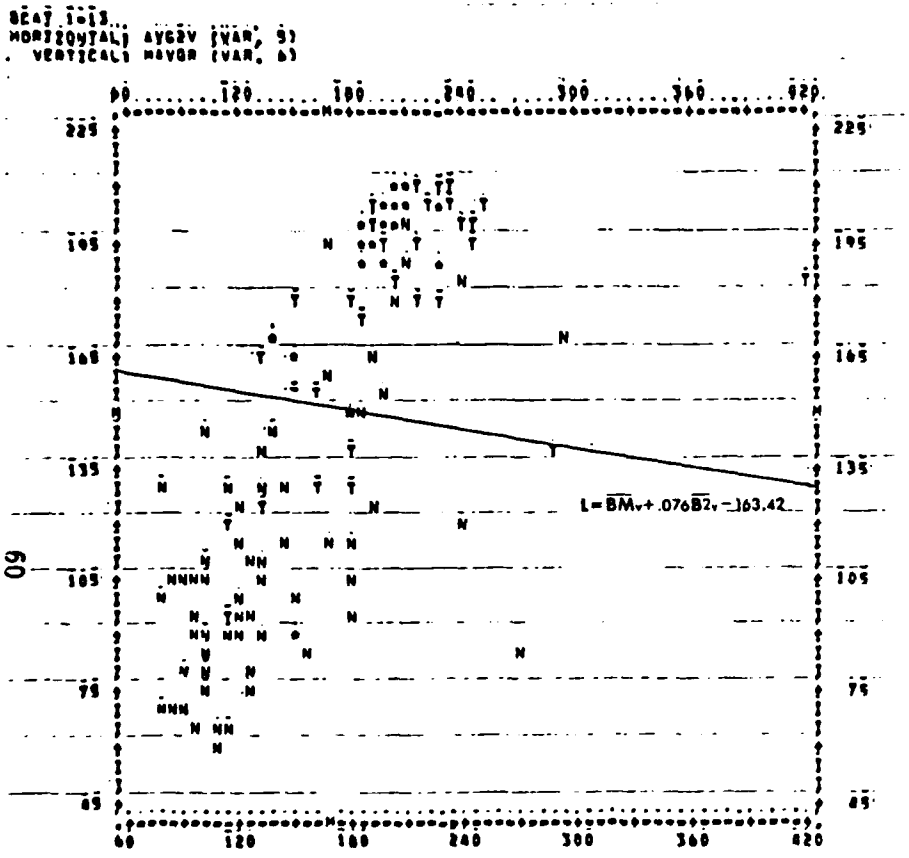
SCAT 1=13
HORIZONTAL: AVG2V (VAR. 5)
VERTICAL: MAVGR (VAR. 6)
L=BM_V+.076B2_V-163.42

H

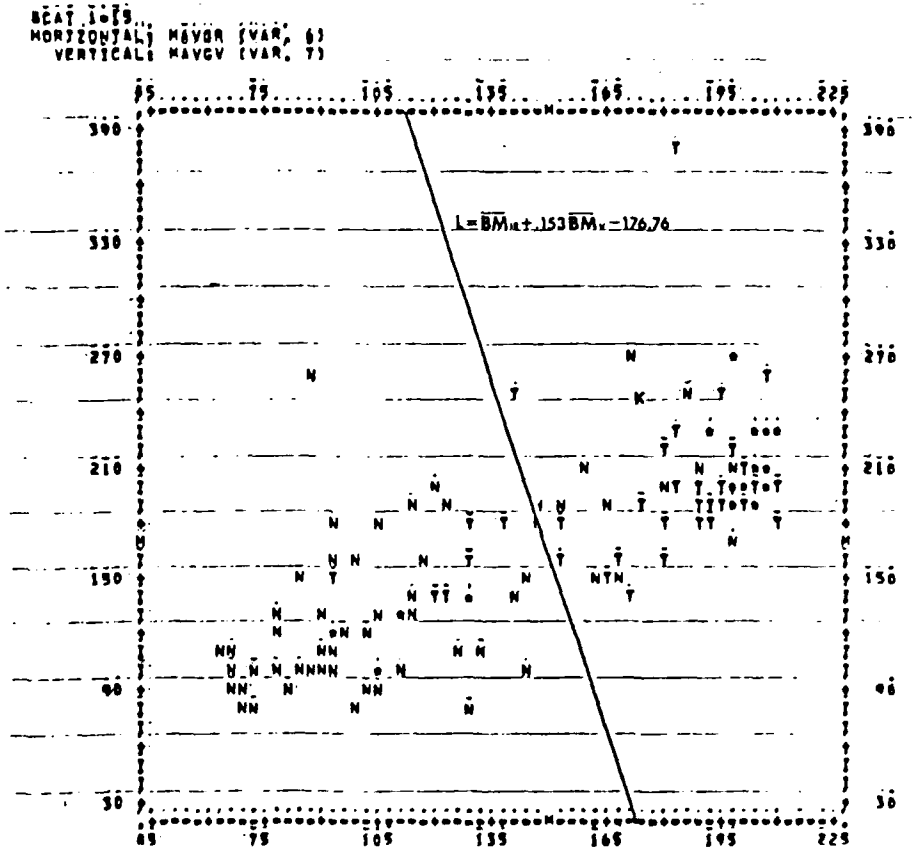
SCAT 1=15
HORIZONTAL: MAVGR (VAR. 6)
VERTICAL: MAVGV (VAR. 7)
L=BM_H+.153BM_V-176.76

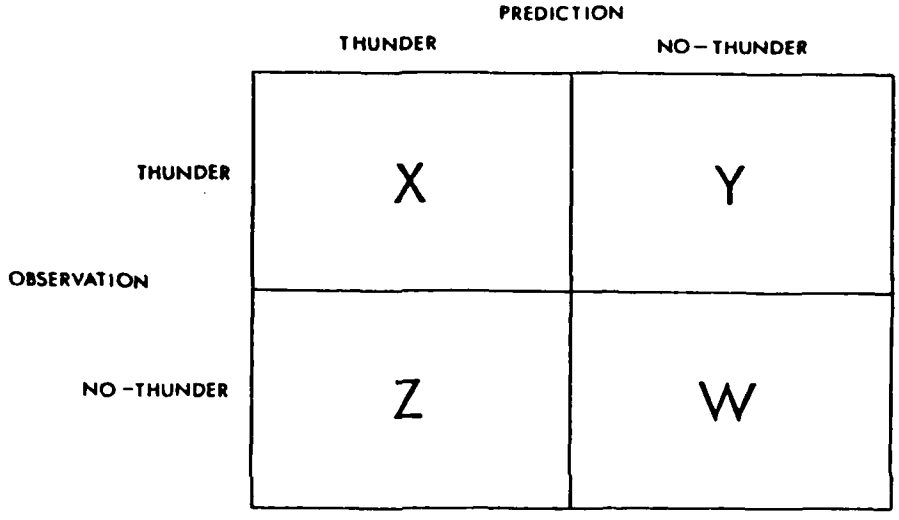

Fig. 6. Contingency table used to determine probability of detection, false alarm ratio, no alarm ratio, and critical success index. See text for further explanation.

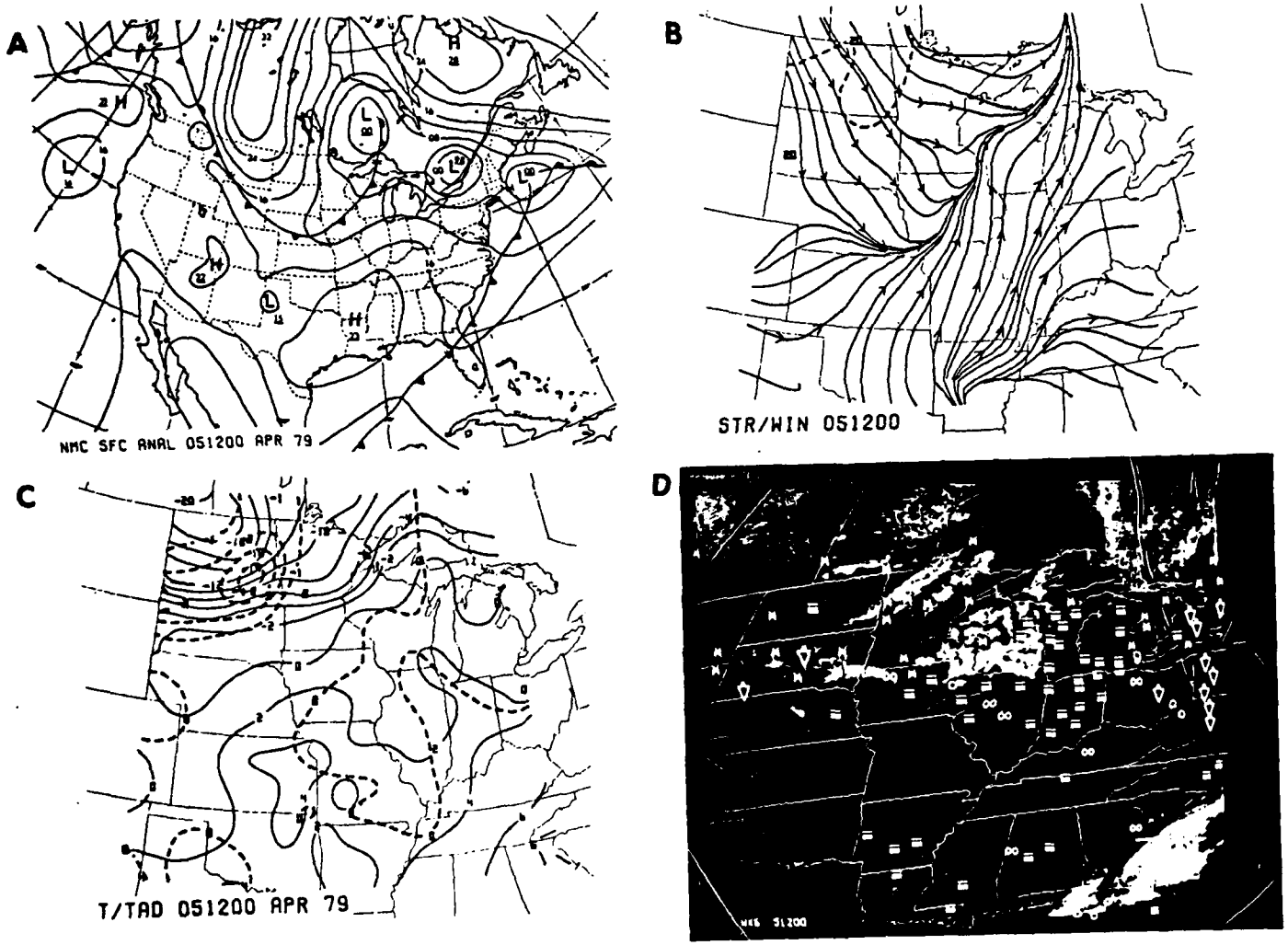

Figure 7. A. NMC MSL pressure analysis for 1200 GMT 5 April 1979.
B. McIDAS streamline analysis for 1200 GMT 5 April 1979.
C. McIDAS analyses of temperature (solid, °C) and temperature advection (dashed, 10°C day^{-1}), for 1200 GMT 5 April 1979.
D. Enhanced GOES IR imagery with superimposed weather symbols for 1200 GMT 5 April 1979.

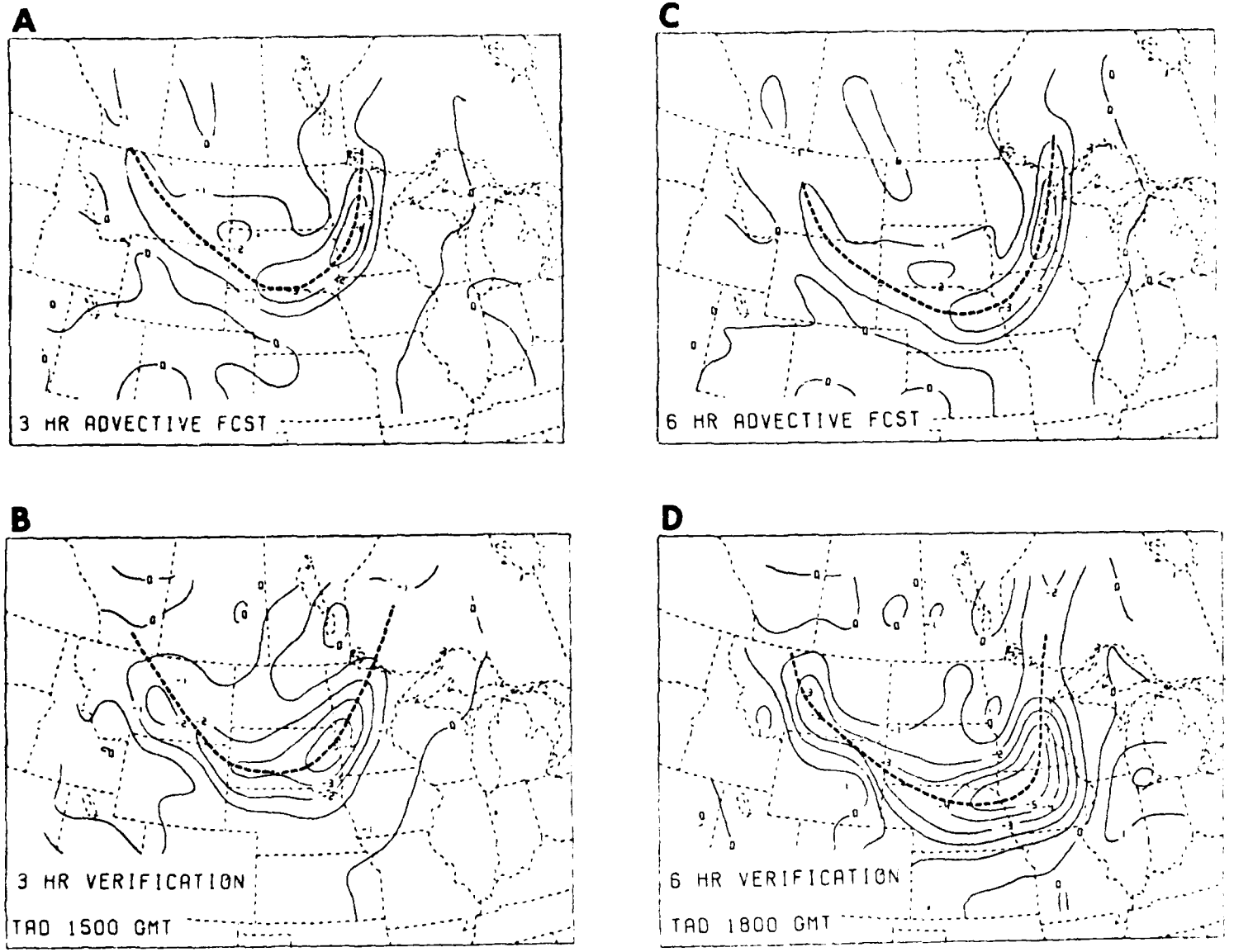

Figure 8. A. 3-hour temperature advection forecast (10°C day^{-1}).
B. Verifying 1500 GMT temperature advection analysis.
C. 6-hour temperature advection forecast.
D. Verifying 1800 GMT temperature advection analysis.

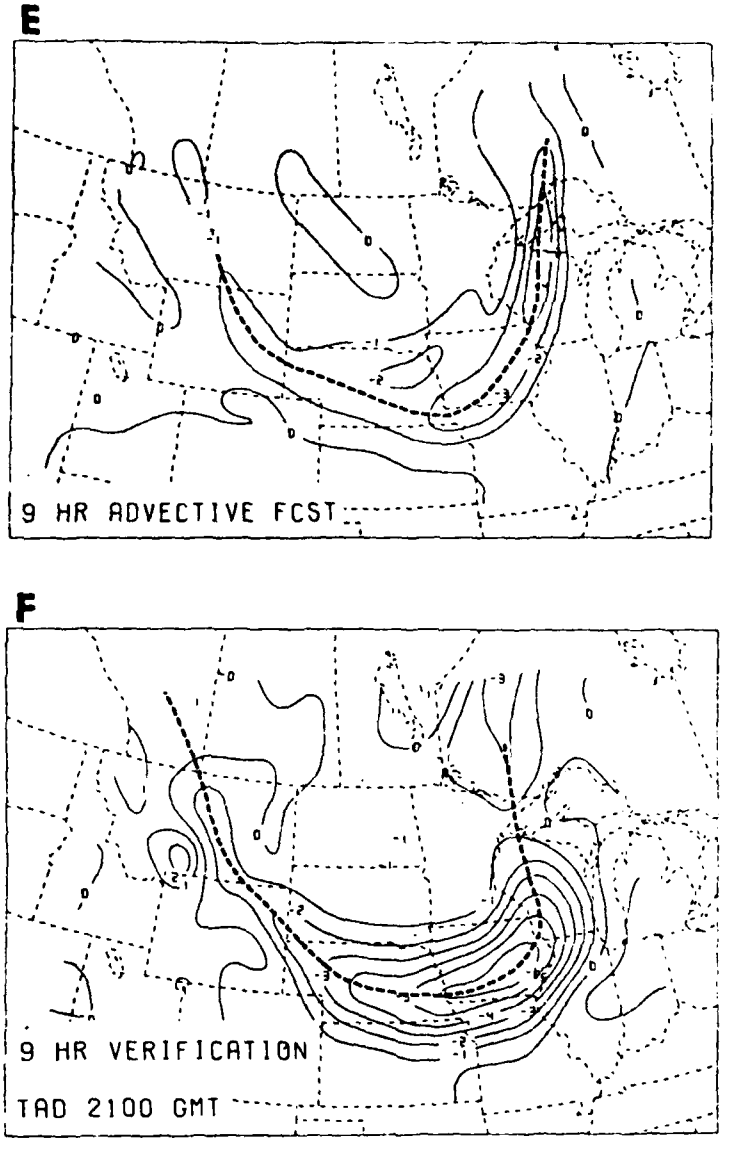

Figure 8. E. 9-hour temperature advection forecast.
F. Verifying 2100 GMT temperature advection analysis.

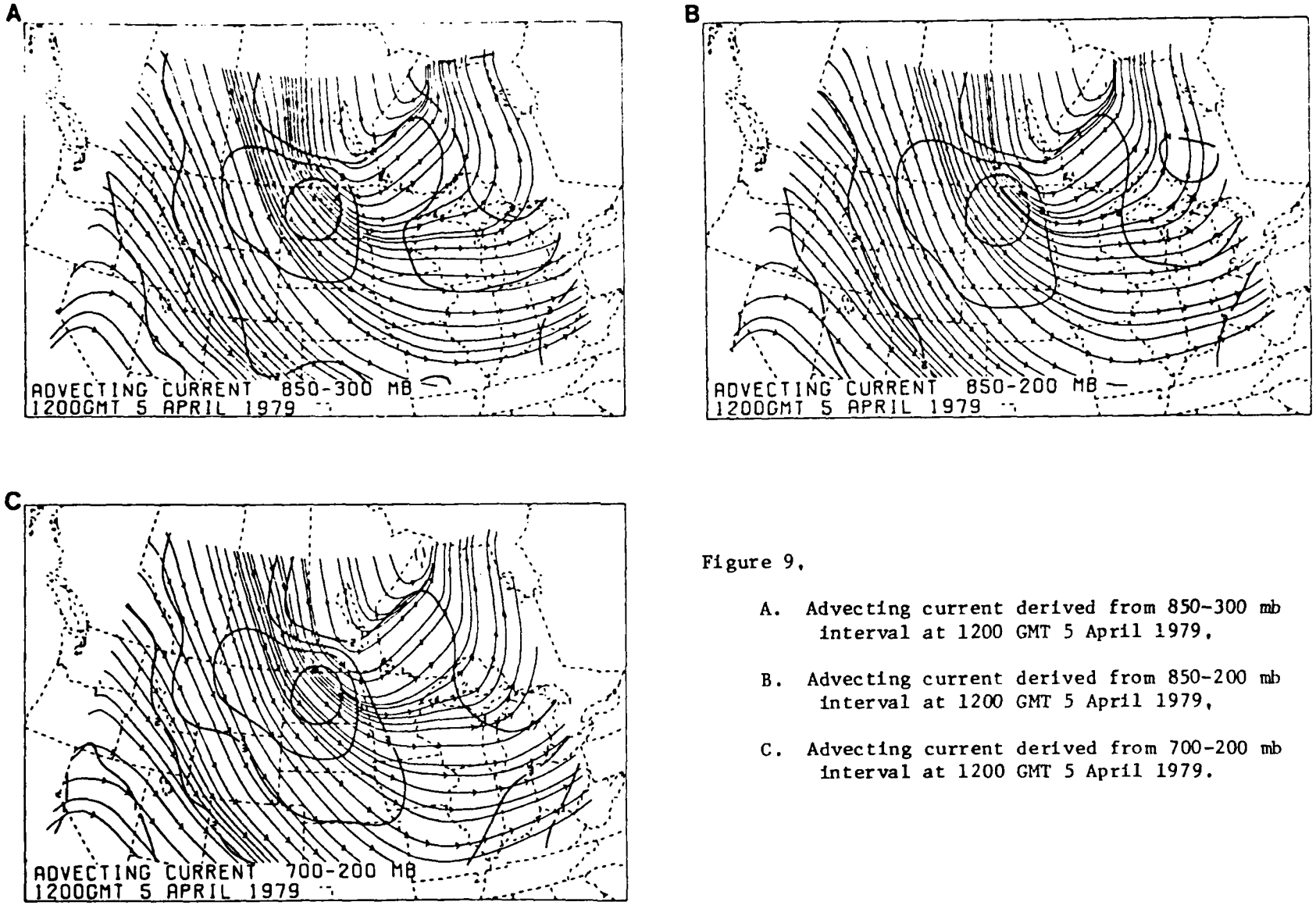

Figure 9,

A. Advecting current derived from 850-300 mb interval at 1200 GMT 5 April 1979,

B. Advecting current derived from 850-200 mb interval at 1200 GMT 5 April 1979,

C. Advecting current derived from 700-200 mb interval at 1200 GMT 5 April 1979.

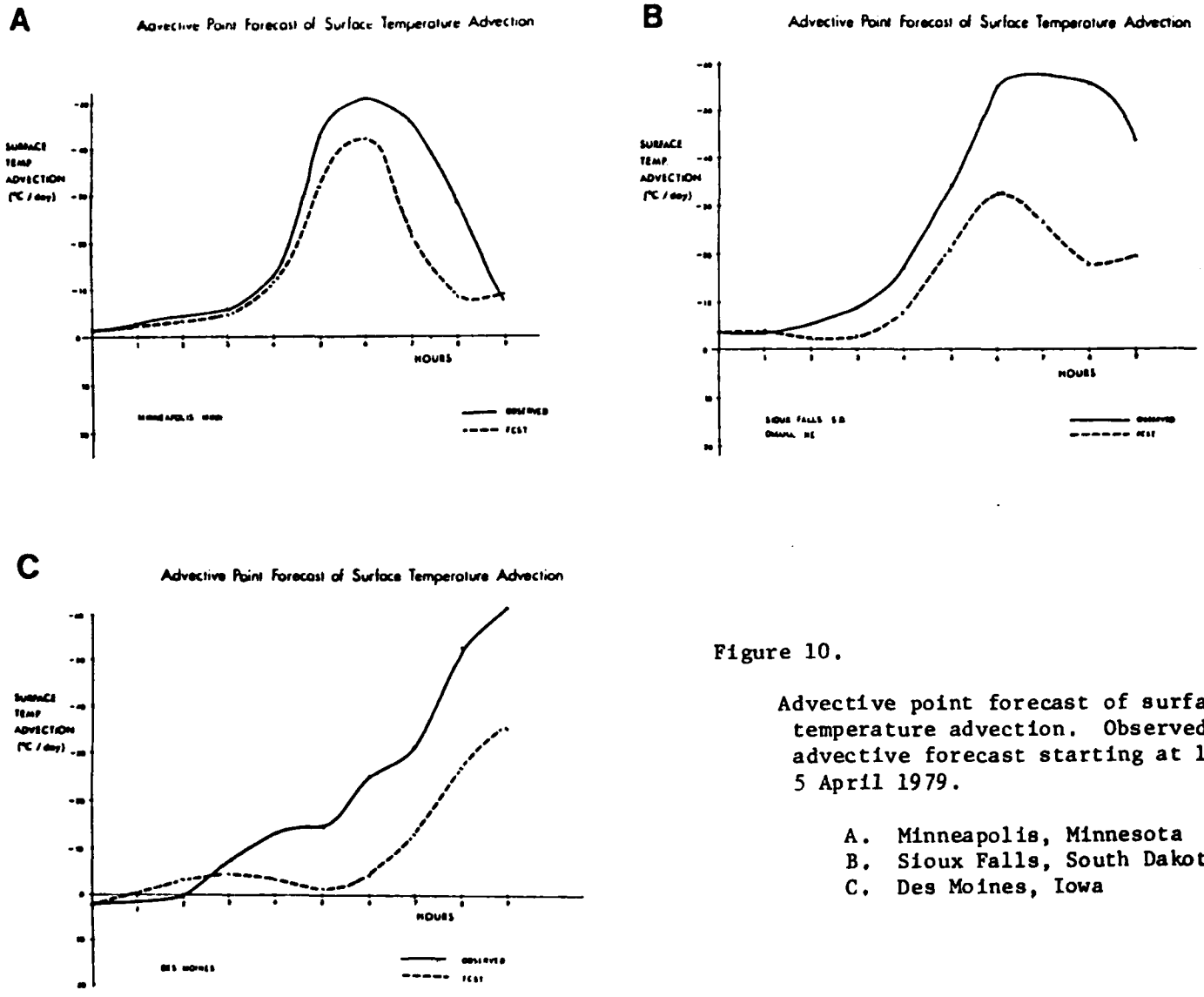

Figure 10.

Advective point forecast of surface temperature advection. Observed vs. advective forecast starting at 1200 GMT 5 April 1979.

A. Minneapolis, Minnesota
B. Sioux Falls, South Dakota
C. Des Moines, Iowa

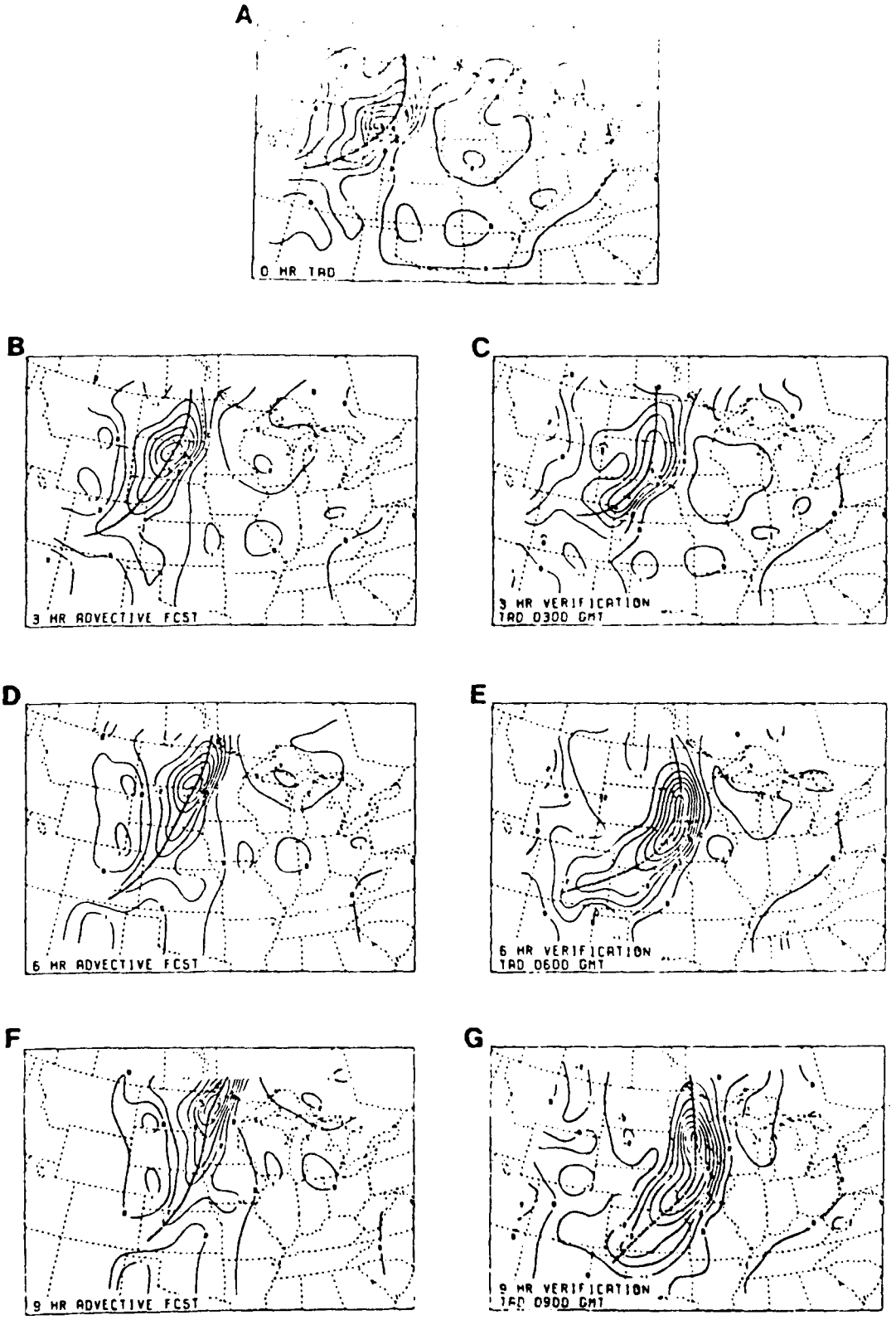

Figure 11. Temperature advection forecasts and verifications for 0000 GMT - 0900 GMT 11 January 1980.

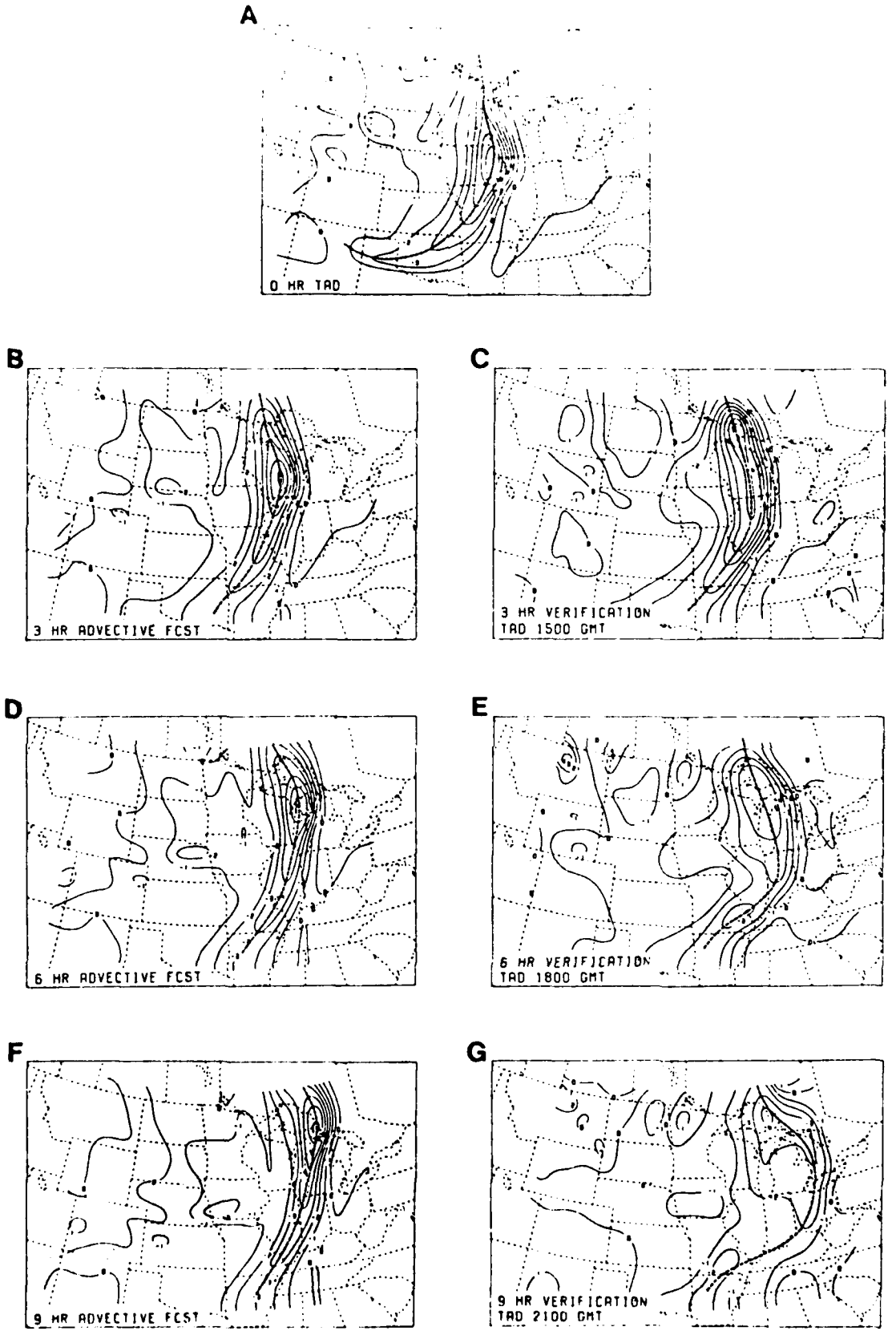

Figure 12. Temperature advection forecasts and verifications for 1200 GMT - 2100 GMT 11 January 1980.

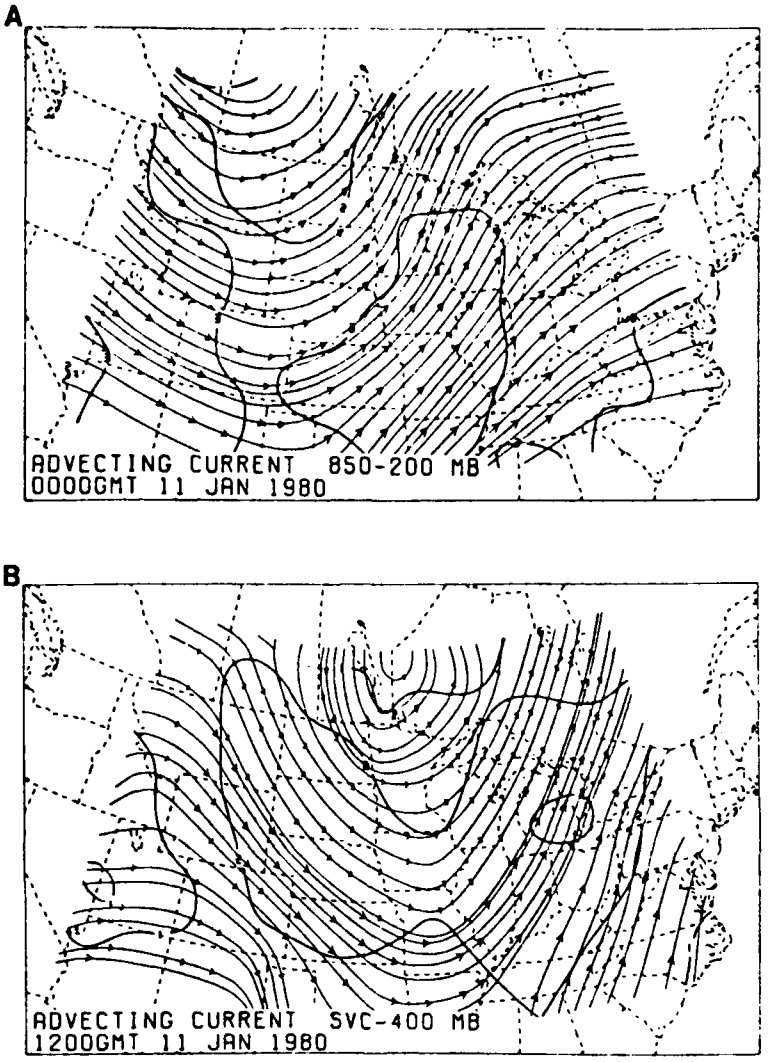

Figure 13. A. Advecting current derived from 850-200 mb interval at 0000 GMT 11 January 1980.

B. Advecting current derived from surface-400 mb interval at 1200 GMT 11 January 1980.

CONTRIBUTING SCIENTISTS, PROGRAMMERS AND GRADUATE STUDENTS

Scientists:	Donald R. Johnson, Principal Investigator
	Carlyle H. Wash
	Delain A. Edman
Programmers:	Thomas M. Whittaker
	Martin Barrett
Graduate Student:	Raymond O'Keefe

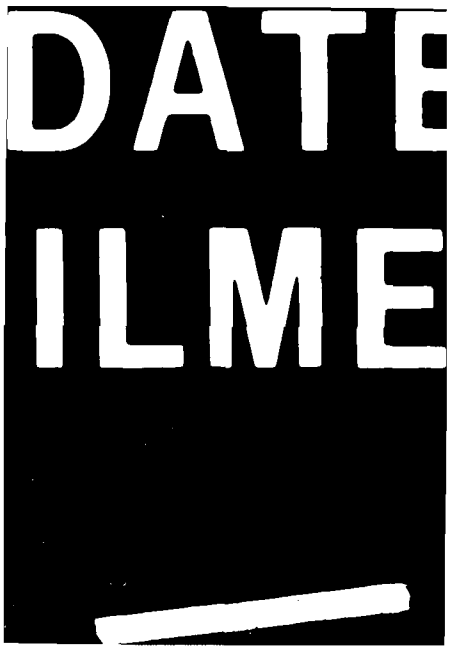
DATE
ILME